Numerical simulation of Orion CEV re-entry vehicle at low altitude

Joseph Pappachan

A Dissertation Submitted to

Indian Institute of Technology Hyderabad

In Partial Fulfillment of the Requirements for

The Degree of Master of Technology

भारतीय प्रौद्योगिकी संस्थान हैदराबाद
Indian Institute of Technology Hyderabad

Department of Mechanical Engineering

July, 2015

Declaration

I declare that this written submission represents my ideas in my own words, and where others' ideas or words have been included, I have adequately cited and referenced the original sources. I also declare that I have adhered to all principles of academic honesty and integrity and have not misrepresented or fabricated or falsified any idea/data/fact/source in my submission. I understand that any violation of the above will be a cause for disciplinary action by the Institute and can also evoke penal action from the sources that have thus not been properly cited, or from whom proper permission has not been taken when needed.

_____

(Signature)

_____

(Joseph Pappachan)

_____

(ME13M1030)

Approval Sheet

This thesis entitled **Numerical simulation of Orion CEV re-entry vehicle at low altitude** by Joseph Pappachan is approved for the degree of Master of Technology from IIT Hyderabad.

(Dr. Narasimha Mangadoddy) External Examiner
Department of Chemical Engineering
IIT Hyderabad

(Dr. Raja Banerjee) Internal Examiner
Department of Mechanical Engineering
IIT Hyderabad

(Dr. K. Venktasubbaiah)Advisor
Department of Mechanical Engineering
IIT Hyderabad

(Dr. Narasimha Mangadoddy) Chairman
Department of Chemical Engineering
IIT Hyderabad

Acknowledgements

Dedicated to my loving Family and Nation

Abstract

Aerothermodynamics analysis of Orion Crew Exploration Vehicle (CEV) re-entry vehicle at low altitude has been studied numerically. At low altitude continuum approximation is valid due to high density region. The Favre averaging (density weighted averaging) procedure is applied to obtain the governing equations. The Favre averaged Navier-stokes along with Spalart-Allmaras turbulent model are used to compute flow field in high density region using open source CFD code SU2 . Results are reported for different Mach numbers, angle of attack and surface temperature. Flow filed characteristics have shown significant change with increases in free stream Mach number. The surface heat flux and surface pressure distribution along the nose radius are reported here. The bow shock strength increases and also forms closer to the surface with increase in Mach number. The surface heat flux drastically changes at the center due to shock/boundary layer interactions. The flow field characteristics significantly changes with increase of angle of attack and surface temperature. Present results matches well with results available in the literature.

Nomenclature

R_n	Nose radius
R	Base radius
K_n	Knudsen number
λ	Mean free path
L	Characteristic length
u,v,w	Velocity components in Cartesian coordinate system
C	Resultant velocity
F	Force per unit mass
μ	Number density
U	Velocity
T	Temperature
ρ	Density
M	Mach number
P	Pressure
T_w	Wall temperature
C_p	Pressure coefficient
S_t	Stanton number
L	Reference length
H	Altitude
Re	Reynolds number
H_0	Total enthalpy
H	Enthalpy
q	Surface heat flux
D	Diameter of re-entry vehicle
μ	Viscosity
α	Free stream condition

Contents

Chapter 1

Introduction

Space exploration is one of the notable and attractive research areas. This research area includes mainly manned and unmanned mission to mars, moon and outer space. One of the giant leaps in the history of mankind was sending man to moon. Now a huge amount of research is going on to find whether human life can sustain in moon and other planets. Mangalyaan, Indian's unmanned mission to mars made India the first Asian country to have an interplanetary orbiter launch to its credit. ISS(International Space Station) a joint venture of five international space agencies is a space station or it can be called artificial satellite of Earth. Lot of research is conducted in ISS mainly in the field of micro gravity, microbial vaccine development, monitoring and forecasting of weather and atmosphere.

1.1 Re-entry Vehicle

Object or vehicle used to deliver people or payload safely through atmosphere of the planet (earth in case of returning) is called re-entry vehicle. A Re-entry Vehicle could be a rocket, satellite, or a manned capsule. When returning to Earth or when landing on another planet, a safe re-entry through the atmosphere is needed. Safe re-entry can be difficult, because the very high speed of the spacecraft creates very high temperatures, when entering through the atmosphere. To enter into Earth's atmosphere sufficient amount of speed is required also. All of this energy used to cross Earth's atmosphere is dissipated mostly in the form of extreme heat according to the conservation of energy principle. At low altitudes the speed of the re-entry vehicle should be less for safe landing also. To design a re-entry vehicle, engineers must study the aerodynamics, deceleration, and trajectory dynamics of the re-entry vehicle. Aerodynamics involves the prediction of forces produced on the vehicle by the atmosphere. Deceleration involves safely reducing the very high speed required for space flight. Trajectory dynamics involves the prediction of the vehicle's motion and steering as it flies through the atmosphere. To dissipate the heat produced during re-entry a suitable thermal protection system is needed.

1.1.1   Thermal Protection System

There are mainly three types of thermal protection system, passive, semi-passive and active thermal protection system. The selection of the thermal protection system depends on the maximum temperature reached and the magnitude and duration of heat produced.

The passive thermal systems are mainly categorized into: heat sink, hot structure and insulated structure. These are very simple and this does not have any moving parts. But the heat dissipating capacity is very less for these systems. Heat sink mainly absorbs the heat incident on it and stores it in usually large metallic mass. But it can be used for short duration heat only. Hot structure radiates most of the heat that are incident on it. It is effective only till the amount of heat radiated is equal to the amount of heat incident on it, after that the temperature will start rising up and the thermal protection system fails. The Inconel X hot structure of the X-15 plane could with stand up to about 922K, which is the maximum temperature for this concept. Insulated structures use and outer shell that radiates most incident heat away from and underlying structure protects by some insulating material. The material used for this purpose is mainly ceramic-fiber batt insulation. All of this thermal protection system can be used when the structure is subjected to heat pulses and up to certain temperature.

There are mainly two types of semi-passive thermal protection system, mainly heat pipes and ablation. Heat pipes are used where there is localized area of high heating and there is adjacent area of low heating. So the heat can be transferred from high temperature area to the low temperature area. The next kind is the ablation. In ablation the ablative material will be coated over the structure. Ablation is a process where the ablative material will sacrifice itself to protect the structure. When the ablative material is exposed to heat, it will absorb the heat to certain temperature and then it will start converting into gas. The conversion of the ablative material to gas is an endothermic reaction, so it will take away the heat with it from the underlying surface. Some of the ablative material used is high temperature reusable surface insulation (HRSI), fibrous Refractory composite insulation tiles (FRCI), toughened unipiece fibrous insulation(TUFI), low-temperature reusable surface insulation (LRSI), flexible insulation blankets (FIB), reinforced carbon-carbon (RCC), nomex felt reusable surface insulation (FRSI) etc.

In active thermal protection system, the cooling water is injected to carry the heat from the surface of the vehicle. The water is circulated at the hot area with the help of the heat exchanger or radiator. The pump, reservoir and heat exchanger will increase the weight to a considerable amount. So the use of this concept is not that much advisable.

The thermal protection system which is used in common is the ablation concept. For selecting the ablative material we need to do know the surface quantities. The surface quantities mainly include temperature, pressure, velocity, heat flux, shear stress etc. Finding these quantities by experimental methods is very difficult and not economical. So the computational methods are used for the prediction of these surface quantities. According to these predictions we will select the material needed and the thickness of the material to be coated on the surface.

1.1.2   History of Re-entry vehicle

The technology needed for re-entry was matured rather quickly in the 1950's. At this time the cold war for ballistic missiles existed between the super powers. The warheads developed during this cold war led directly to the capsules which allowed humans to enter into space. The short range ballistic missiles were first tested by Germany under the guidance of Wernher von braun. The working vehicle was named Assembly-4(A4). But it reached only up to an altitude of 50 to 60 miles(80.47 to 96.56 kms) and to a maximum velocity of Mach 4 and a distance of 200 miles(627.44 km). Aluminum alloys and conventional steel were used, the temperature it experienced while travelling through the earth's atmosphere was well within its heat and strength capacity [1].

In 1953, this same team made another ballistic missile which flew higher and carried more payloads; it reached to a velocity of maximum velocity of Mach 5.5 during re-entry. They made improved version of this named Jupiter which reached up to a height of 390 miles (627.44 km), maximum velocity of Mach 15 during its re-entry and reached a maximum range of 1500 miles (2414 km). After this came the X plane series, X-15 aircraft was designed which flown more than Mach 6 and above 30000 feet. X-15 project testing gave lot of data that became useful for the design of aircraft and spacecraft. X-15 reached up to a maximum sped of 4,520 miles per hour [2].

President of US Eisenhower signed the National Aeronautic and space act of 1958 and assigned the nation's humans space flight mission to NASA. It was having two goals: send the human I orbit around the earth and also should be done before the Soviet Union. After this assignment NASA started project Mercury, project continued from 1959 to 1963.They succeeded on May 1961 and Alan Shepard became the first American in space. They used a blunt body re-entry vehicle for Mercury project. The ablative material used as the thermal protection system was beryllium or ablative fiberglass. After re-entry parachute was deployed and the landing was on sea water [3].

3

On the same year 12 April 1961, The Vostok spacecraft of Union Soviet Union put Yuri Gagarin in outer orbit and became the first person to travel in space. Re-entry vehicle shape of the Vostok was spherical and it required the thermal protection from all side.

Project Gemini was the second human spaceflight program of NASA and it was modified version of project mercury. It performed ten manned flights occurring in 1695 and 1966. Project Gemini was made to put two-man in space followed by one in Mercury[4].

Project Apollo started with US President John F Kennedy's national goal of "landing a man on the Moon and returning him safely to the Earth" in 1968. Apollo space craft designs were extension of Mercury and Gemini project of blunt shape and thermal protection system based on ablation process using Avcoat, a glass filled epoxy-novalc system. On July 20, 1969 Apollo 11 successfully accomplished Kennedy's goal when astronauts Neil Armstrong and Buzz Aldrin landed on lunar surface. In between 1968 to 1972 six Apollo spaceflights were done and 12 men walked on the Moon [5].

Apollo module was further used for three missions of Skylab, United states first space station between 1973 and 1974 and re-entry on earth in 1979. After that other space laboratory started by NASA in 1983 and 22 shuttle mission were done from 1983 to 1988. Russia built space station Mir in between 1986 to 1996 and Soyus, a modified version of Vostok used as primary re-entry vehicle and after that Mir shuttle used as re-entry vehicle.

International Space Station (ISS) work started as joint venture of five space agency in 1998. Russian space craft Soyuz and Progress space craft, European Space Agency (ESA) unmanned space craft named Automated Transfer vehicle (ATV), Japanese's unmanned space craft H-11 Transfer vehicle used for delivery of man and payload to ISS. Orion, a NASA next generation space craft will also serve mission to ISS.

Space shuttle type re-entry vehicle with wings are easy landing on run ways as plane and also reusable but their use limited up to lower orbit of earth. Space shuttle are designed only up to 17500 mph (28163.52 km/h) to go outside of the earth gravitation. Entering the Earth's atmosphere at this high speed would destroy the shuttle because it would exceed the wing and fuselage load limits. Currently, there is no thermal protection system that would protect the wings from such a high heat load. The space craft is preferred than space shuttle to enter the orbit due to more load capacity , higher speed and better thermal protection system.

The Indian manned spacecraft temporarily named Orbital Vehicle is intended to be the basis of the indigenous Indian human spaceflight program by ISRO. The capsule will be designed to carry three people, and a planned upgraded version will be equipped with

rendezvous and docking capability. However the future of the project is in doubt due to funding problems and numerous technical challenges.

Country	Agency	Vehicle	Mission
United states	National Aeronautics and Space Administration(NASA)	Orion	Mars, Moon, ISS
Russia	Russian Federal Space Agency	Soyuz	ISS
Europe	European Space Agency(ESA)	Automatic Transfer Vehicle(ATV)	`ISS
Japan	Japan Aerospace Exploration Agency(JAXA)	H-II Transfer Vehicle(HTV)	ISS Unmanned
China	China National Space Administration(CNSA)	Shenzhou	
India	|Indian Space Research Organization (ISRO)	Orbital Vehicle(OV)	

1.1.3 Orion CEV

The project Orion Crew Exploration Vehicle (CEV) was defined by NASA's Exploration Systems Architecture study in 2005 for NASA's next manned space vehicle [6]. The CEV will support NASA's exploration missions by providing crew access to the International Space Station, the moon, and Mars. The geometry of Orion CEV is similar to that of Apollo but larger in size and mass is almost double of Apollo. The Orion Crew Module will hold four to six crew members, depending on the type of mission: the LEO version will be able to carry six crew members to the International Space Station, while the lunar and Mars versions would carry a crew of four and six members respectively. Although it may have an Apollo shape, the new spacecraft will have significant advances including:

Service Module   Crew   Launch Abort
                  Module   System (LAS)

Figure 1.1: Orion spacecraft

- The safest most efficient shape for going beyond low Earth orbit
- Advanced materials, avionics and manufacturing process.
- Computers and the experience gained from 40 years of human space flight
- Increased volume. It can carry more crew and cargo
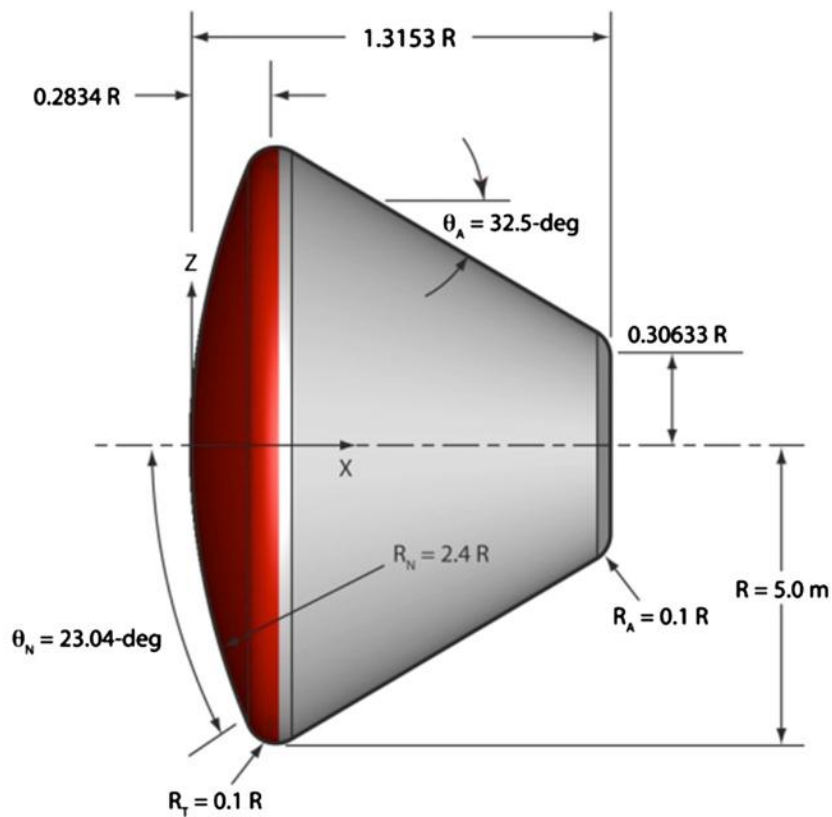- Improved operational efficiency and overall capability in a vehicle shaped much like the original Apollo capsule.

Figure 1.2: Schematic diagram of Orion CEV

Heat load during the Orion re-entry is very high therefore thermal protection system of Orion will done by semi passive ablation process. Avcoat and PICA (Phenolic Impregnated Carbon Ablator) will be used as ablator for Orion CEV heat shield. Recovery of Orion CEV will be done by landing on sea water with help of parachutes.

1.2 Literature Survey

The re-entry vehicle enters Earth's atmosphere at high speed, a lot of heat will be produced while it travel through Earth's atmosphere. A bow shock will be formed in front of the re-entry vehicle and a lot of heat will be produced due to the aerodynamic heating. So for the design purpose of re-entry vehicle we need to know the surface quantities that are produced, mainly heat flux, temperature, pressure, shear stress etc. We can select the ablative material for the thermal protection system only after predicting these surface quantities. The prediction of these surface quantities by experimental methods are very costly and time consuming. So we go for the computational methods for finding the surface quantities during re-entry.

In the literature blunt shape of re-entry vehicle was proposed by Allen[7] and Eggers[8] and their work in the history considered as pioneer work in the field of hypersonic flows. They pointed out that the blunt shape was optimum for relatively light weight re-entry bodies.

History of hypersonic flow were given by Heppenheimer[9]. Moretti and Abbetti [10] numerically studied the supersonic flow over blunt body. Betin and Cummings [11] reported the progress of research in the field of hypersonic flows in the last fifty years. In the literature, the aerodynamics of the blunt body entry vehicles Hollis and Borelli [12] is discussed. Four topics are discussed in it mainly turbulent flow, non-equilibrium flow, rarefied flow and radiation transport. Examples of comparisons between computational tools to ground and flight-test data will be presented in order to illustrate the challenges existing in the numerical modelling of each of these phenomena and to provide test cases for evaluation of computational fluid dynamics (CFD) code predictions. In the discussion of blunt-body aero thermodynamic phenomena, ground and flight test programs and supporting computational analyses will be discussed for several programs: the Mars Science Laboratory, the Orion Crew Exploration Vehicle, and the Fire II flight test. In this literature he has given the schematic diagram of Orion Crew Exploration. Turbulent aero heating

testing of the Orion CEV vehicle was conducted in the Calspan University of Buffalo Research Centre (CUBRC) Large Energy National Shock Tunnel (LENS) I Hypervelocity Reflected Shock Tunnel. Laminar and turbulent perfect-gas comparisons to these data were performed using the LAURA code with the algebraic Cebeci–Smith turbulent model being used for the turbulent cases. Data needed for validation are taken from this literature.Computational flow field analysis of blunt body re-entry vehicle was reported by viviani [13]. He has solved the Euler and Navier-stokes equations with the assumption of low orbit re-entry scenario. Pezzella [14] reported the aerodynamic and aero thermodynamic trade-off analysis for configuration design of re-entry vehicle. Stella et al. [15] reported the flow field around YES-2 re-entry capsule using CFD. They have used a simplified model based on modified specific heats to account the dissociate effects. Pezzella [16] have studied the hypersonic environment assessment of the FTB-X re-entry vehicle. He has considered the air as a perfect gas model and analyses are based on laminar flow conditions. Ohtake [17] have studied the thermal analysis of thermal protection system for the re-entry vehicle. He has performed flow and structure analysis using Finite element methods. Savino et al. [18] studied the thermal analysis of thermal protection system for the re-entry vehicle. They have investigated the thermal response of ultra-high temperature ceramics (UHTC) material for thermal protection system of re-entry vehicle.

A hypersonic vehicle, entering an atmosphere, will go through many different flow regimes due to the change in atmospheric density with altitude. At lower altitudes where the density is high and the Knudsen number is low, flows should be simulated using traditional computational fluid dynamics (CFD) techniques by numerically solving the Navier-Stokes equations. However, when the Knudsen number becomes larger, the continuum assumption in the Navier-Stokes equations starts to breakdown. At higher altitudes, in the rarefied flow regime, only a non-continuum technique can be used, such as the classical Direct Simulation Monte Carlo (DSMC) method that is particle method for simulating non-equilibrium gas flows.

Aerothermodynamics analysis of the Orion CEV re-entry vehicle at high altitude has been studied numerically in the paper [19]. At high altitude in the rare field flow regime non continuum technique such as direct simulation Monte Carlo (DSMC) method is used to solve the Boltzmann equation of kinetic theory. Results are reported at different altitudes in the rare field regime for ideal gas and real gas model. The effects of nose radius and free stream velocity are presented. The estimation of bow shock strength and peak surface heat flux is higher for ideal gas compared with real gas model. The flow field characteristics

have shown significant change with decrease in altitude and increase in the free stream velocity.

1.3 Motivation

Orion CEV is future human exploration vehicle and it is in design phase. Very few numerical studies on Orion CEV re-entry vehicle at low altitude were reported earlier. The present investigation has been motivated for the following points. (i) Detailed analysis of aerothermodynamics of Orion CEV re-entry vehicle at low altitude for different mach number (ii) Effect of angle of attack (iii) Effect of wall temperature are not available in the literature.

1.4 Objectives

The main objective of present work is to study the flow field characteristics and estimation of maximum heat flux around Orion CEV re-entry vehicle in high density regime at low altitude.

- Effect of Mach number
- Effect of angle of attack
- Effect of wall temperature

1.5 Outline of the thesis

- Chapter 2 gives the description about the governing equations and numerical method for high density region.
- Chapter 3 deals with grid independency test, validation and results and discussion in high density region.
- Chapter 4 is Conclusion and
- Chapter 5 is Scope of Future work.

Chapter 2

Formulation and Numerical methods

2.1 Formulation in high density region at low altitude

Governing Equations

The governing equations are derived from conservation laws and the first law of thermodynamics. The governing equations comprising the unsteady Favre averaged Navier-Stokes equations including the time average energy equation for temperature field. Turbulence modeled by Spallart-Allmaras model.

The conservation equations for turbulent compressible flows are as follows:

Continuity equation:

Conservation of mass states that the total mass of the universe is constant; in other words, mass is neither created nor destroyed but can only be moved from one place to another.

$$\frac{\partial \rho}{\partial t} + \frac{\partial}{\partial x_j}\left[\rho u_j\right] = 0 \qquad \text{j=1, 2, 3} \tag{2.1}$$

Momentum equation:

Conservation of momentum says that momentum changes due to one of three factors-redistribution, conversion of momentum to or from energy and force. In other words, if momentum increases in one place, either momentum or an equivalent amount of energy must decrease someplace else, or a force must act.

$$\frac{\partial}{\partial t}(\rho u_i) + \frac{\partial}{\partial x_j}\left[\rho u_i u_j + p\delta_{ij} - \tau_{ji}\right] = 0, \qquad \text{i, j =1, 2, 3} \tag{2.2}$$

Energy equation:

Conservation of energy says that energy change is due to one of three factors redistribution, conversion of energy to or from momentum, or conversion to or from some other form of energy, heat, or work. In other words, if energy increases in one place, either energy or an equivalent amount of momentum must decrease someplace else, or heating or work must be done.

$$\frac{\partial}{\partial t}(\rho e_0) + \frac{\partial}{\partial x_j}\left[\rho u_j e_0 + u_j P + q_j - u_i \tau_{ji}\right] = 0 \qquad \text{i, j= 1, 2, 3} \qquad (2.3)$$

Viscous stress is given by:

$$\tau_{ij} = 2\mu S_{ij}^*, \qquad \text{i, j= 1, 2, 3} \qquad (2.4)$$

Where the viscous strain rate is defined by,

$$S_{ij}^* = \frac{1}{2}\left(\frac{\partial \rho u_i}{\partial x_j} + \frac{\partial u_j}{\partial x_i}\right) - \frac{1}{3}\frac{\partial u_k}{\partial x_k}\delta_{ij}, \qquad \text{i, j= 1, 2, 3} \qquad (2.5)$$

Where $\mu = u_l + \mu_t$ is the total viscosity; μ_l, μ_t being the laminar and turbulent viscosity.

Laminar viscosity (μ_l) is calculated from Sutherland's law as,

$$\mu_l = \mu_{ref}\left(\frac{T}{T_{ref}}\right)^{\frac{3}{2}}\frac{T_{ref}+S}{T+S} \qquad (2.6)$$

T_{ref} is a reference temperature

μ_{ref} is the viscosity at the T_{ref} reference temperature

S is the Sutherlands Coefficient.

Specific as function of temperature for air is given by,

For 200≤ T< 1000

$$C_p = 1161.482 - 2.368814T + 0.01485511T^2 + -2.034909 \times 10^{-5}T^3 + 9.928569 \times 10^{-8}T^4 - 1.111097 \times 10^{-10}T^5$$

For 1000≤ T <3000

$$C_p = -7069.814 + 33.70605T - 0.0581276T^2 + 5.421615 \times 10^{-5}T^3 - 2.936676 \times 10^{-8}T^4 + 9.237533 \times 10^{-12}T^5$$

And,

$$\Upsilon = \frac{C_p}{C_v} \qquad (2.7)$$

$$P = \rho RT \qquad (2.8)$$

The Spalart-Allmaras turbulent model is a relatively simple one-equation model that solves a modeled transport equation for the kinematic eddy(turbulent) viscosity. This embodies a relatively new class of one-equation models in which it is not necessary to calculate a length scale related to the local shear layer thickness. The Spalart-Allmaras model was designed specifically for aerospace applications involving wall-bounded flows

and has been shown to give good results for boundary layers subjected to adverse pressure gradients. It is also gaining popularity in the turbo machinery applications.

The model proposed by Spalart and Allmaras solves a transport equation for a quantity that is a modified form of the turbulent kinematic viscosity.

The transported variable in the Spalart-Allmaras model, $\bar{v}$,is identical to the turbulent kinematic viscosity except in the near-wall(viscosity-affected) region. The transport equation for $\bar{v}$ is,

$$\frac{\partial}{\partial t}(\rho\bar{v}) + \frac{\partial y}{\partial x_i}(\rho\bar{v}u_i) = G_v + \frac{1}{\sigma_{\bar{v}}}\left[\frac{\partial}{\partial x_j}\left\{(\mu + \rho\bar{v})\frac{\partial\bar{v}}{\partial x_j}\right\} + C_{b2}\rho\left(\frac{\partial\bar{v}}{\partial x_j}\right)^2\right] - Y_v + S_{\bar{v}}$$

(2.9)

where G_v is the production of turbulent viscosity and Y_v is the destruction of turbulent viscosity that occurs in the near-wall region due to wall blocking and viscous damping. $\sigma_{\bar{v}}$ and C_{b2} are the constants and v is the molecular kinematic viscosity. $S_{\bar{v}}$ is a user-defined source term. Note that since the turbulence kinetic energy k is not calculated in the Spalart-Allmaras model, while the last term in equation is ignored when estimating the Reynolds stresses.

The turbulent viscosity μ_t is computed from,

$$\mu_t = \rho\bar{v}f_{v1}$$

(2.10)

Where the viscous damping function f_{v1} is given by,

$$f_{v1} = \frac{X^3}{X^3 + C_{v1}^3}$$

(2.11)

and

$$X = \frac{\bar{v}}{v}$$

(2.12)

The destruction term is modelled as,

$$Y_v = C_{w1}\rho f_w\left(\frac{\bar{v}}{d}\right)^2$$

(2.13)

where

$$f_w = g\left[\frac{1 + C_{w3}^6}{g^6 + C_{w3}^6}\right]^{\frac{1}{6}}$$

(2.15)

$$g = r + C_{w2}(r^6 - r)$$

(2.16)

$$r = \frac{\bar{v}}{Sk^2d^2}$$

(2.17)

$$\bar{S} = S + \frac{\bar{v}}{k^2d^2}F_{v2}$$

(2.18)

$$f_{v2} = 1 - \frac{X}{1+Xf_{v1}} \tag{2.19}$$

C_{b1} and k are constants, d is the distance from the wall, and S is a scalar measure of the deformation tensor as proposed by Spalart and Allmaras. S is based on the magnitude of the vorticity,

$$S = \sqrt{2\Omega_{ij}\Omega_{ij}} \tag{2.20}$$

where Ω_{ij} is the mean rate-of-rotation tensor and is defined by

$$\Omega_{ij} = \frac{1}{2}\left(\frac{\partial u_i}{\partial x_j} - \frac{\partial u_j}{\partial x_i}\right) \tag{2.21}$$

Corresponding constants are given by,

$$C_{b1} = 0.1355$$
$$C_{b2} = 0.622$$
$$\sigma_{\bar{v}} = \frac{2}{3}$$
$$C_{v1} = 7.1$$
$$C_{w1} = \frac{C_{b1}}{k^2} + \frac{(1+C_{b2})}{\sigma_{\bar{v}}}$$
$$C_{w1} = 0.3$$
$$C_{w2} = 2.0$$
$$k=0.4187$$

2.2 Numerical Method for high density region

2.2.1 Geometry and meshing

The geometry was made with the help of solid edge software and the meshing was done using Pointwise software. Geometry was saved in igs format and exported to Pointwise software. Meshing was done by the extrusion method. The initial spacing near the re-entry vehicle was about 2.35e-5 and a growth rate of 1.2 is given for the geometric progression. Upstream length is about 50 times of the nose radius and the downstream length is about 150 times of the nose radius. Meshes developed are structured meshes and they are tetrahedron in shape. A total of 41712 grids are generated. The boundary conditions are given as farfield for the domain and the wall condition for the re-entry geometry. The mesh can be directly saved in su2 format or it can be saved in cgns format and the su2 software will convert it into the su2 format.

2.2.2 CFD Software

The numerical simulation was done using SU2 (Stanford University Unstructured). The SU2 suite is an open-source collection of C++ based software tools for performing Partial Differential Equation (PDE) analysis and solving PDE constrained optimization problems. The toolset is designed with computational fluid dynamics and aerodynamic shape optimization in mind, but is extensible to treat arbitrary sets of governing equations such as potential flow, electrodynamics, chemically reacting flows, and many others. SU2 is under active development in the Aerospace Design Lab (ADL) of the Department of Aeronautics and Astronautics at Stanford University, and is released under an open-source license.

SU2 is able to run on any computing platform which has C++ compiler. Both Finite Volume Method (FVM) and FEM approach can be done in SU2. SU2 is under active development in the Aerospace Design Lab (ADL) of the Department of Aeronautics and Astronautics at Stanford University. It is also under open source license, it is freely available and developers anywhere can change the codes, and improve the suite.

The inputs for the SU2 software are mesh file and configuration file.

Mesh file: SU2 uses its own mesh format .su2, it takes cgns format also. SU2 converts CGNS format to SU2 format before simulation. SU2 is capable of analyzing two dimensional and three dimensional problems also. So the first thing specified in this mesh is NDIME, which can be set to either 2 or 3, depending on the dimension of the specified problem. The numbers of elements are denoted by NELEM and the boundaries by MARKER_TAG. Here we are giving a two dimensional problem, the number of elements are around 42000 and the number of markers are two.

Configuration file: To assign solvers, specify boundary conditions and other conditions necessary for a simulation, the correct options have to be set in SU2 configuration file .cfg. In SU2 most specifications are already assigned by default. In the configuration file these default values can be changed. The time discretization, viscous terms discretization, convective terms discretization, linear solvers and convergence criterion are given in this configuration file. The boundary conditions given are farfield boundary conditions to the domain and wall boundary conditions to re-entry vehicle. Spalart-Allmaras turbulent model is used. We give Mach number, Reynolds number, Reynolds length and free stream temperature in the configuration file, with free stream temperature and the gas constants the solver will find the free stream velocity from the Mach number relation. Using the Sutherland's law the dynamic viscosity is calculated using the free stream temperature.

Density is calculated using ideal gas equation and using these entire values solver will find the density from the Reynolds number formulae.

The output files can be post processed with the help of Paraview and tecplot. There are provisions for restarting the solutions. Parallel running also can be done with SU2 software. SU2 is one of the open source software which is under mammoth development and it will become more sustainable in the near future.

2.2.3   Post Processing

Post processing was done using tecplot. Tecplot software empowers engineers and scientists working with computational fluid dynamics (CFD) to discover, analyze, and understand information in complex data. WebplotDigitizer was used to extract data from the paper to validate the results.

Chapter 3

Results and discussion

3.1 Grid Independency test

To check that there is no effect of grid sizes on the numerical solution results, Grid independency test is performed. Grid independence test is performed with four different mesh sizes. The operating free stream conditions are given below:

Table 3.1: Operating conditions for grid independency test

Angle of attack	0 degree
Reynolds number	10.072178E8
Mach number	7.80
Pressure	8290 Pa
Temperature	74.1 K
Density	0.378 kg/m3
Velocity	1367 m/s

Meshes are generated with four different grid sizes 42000 cells, 49000 cells, 55000 cells and 62000 cells. The pressure distribution on the nose radius of re-entry vehicle is plotted in Fig 3.1. It is clear that the pressure distribution on the nose radius of the re-entry vehicle overlap each other. Quantitative comparison of the maximum surface pressure on the nose for four grids is shown in Table 3.2. It can be seen that the solution is grid independent and there is very less variation in the performance of the different grids. Hence all simulations are performed with 41712 cells.
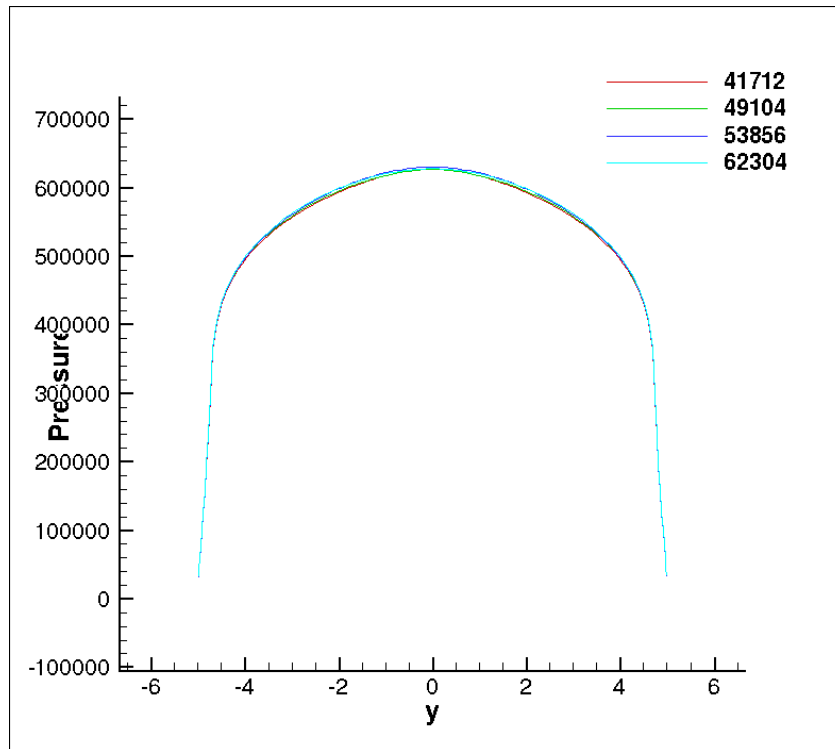
Figure 3.1: Pressure(Pa) distribution along the nose radius with different grids

Table 3.2: Comparison of maximum pressure at the surface.

Number of grids	Maximum pressure (kPa)
41712	628.0249
49104	627.0792
53856	630.7456
62304	628.1575

.

3.2 Validation

Study of external flow over a re-entry vehicle involves the aerodynamics, thermodynamics analysis. Computational fluid dynamics (CFD) being one of the most powerful tools for understanding various flow phenomena and helps in analysing the flow field physics and helps in designing and analysis of the re-entry vehicle guiding control and thermal protection system (TPC). The present numerical methods are validated with the experimental work of Hollis and Bergar et al.[12] Experimental work on 0.035 scale model of Orion CEV vehicle was done at Arnold Engineering Development Centre (AEDC) hypersonic wind tunnel No.9 for Mach 8 and Mach 9. From their experimental work test case is selected for comparison of present numerical method in high density region. Case selected is named as RUN 3076 with perfect nitrogen as fluid flow. Operating condition of these cases is given in Table 3.3. They measured thermal heating fore body of Orion vehicle as $St * Re^{\left(\frac{1}{2}\right)}$, and it is defines as,

$$St * Re^{\left(\frac{1}{2}\right)} = \frac{q}{\rho C_p U_\alpha (T_W - T_o)} * \left(\frac{\rho v l}{\mu}\right)^{\left(\frac{1}{2}\right)}$$

Table 3.3: CEV test conditions for AEDC Tunnel

Reynolds number	10.072178E8
Mach	7.80
Angle of Attack	28.0
Pressure	8290 Pa
Temperature	74.1 K
Density	0.378 kg/m3
Velocity	1367 m/s

Numerical simulations are performed with same operating conditions on 0.04 scaled model of Orion CEV re-entry vehicle. Two dimensional unsteady compressible equations with Spalart- Allmaras turbulent modeling are solved. Results of present simulations are

18

presented in terms of Staton number variation on the fore body (nose radius) of Orion CEV at steady state is considered in the wind side.   From Fig: 3.2, we can notice that the minimum value of $St * Re^{\left(\frac{1}{2}\right)}$ is near to the flow incident point due to stagnation condition; here the heat transfer is also minimum.

$$St * Re^{\left(\frac{1}{2}\right)} = \frac{q}{\rho C_p U_\alpha (T_w - T_o)} * \left(\frac{\rho v l}{\mu}\right)^{\left(\frac{1}{2}\right)}$$

Mach, Pressure and Temperature contours are shown in the Fig. 3.2, 3.3 and 3.4 respectively. Bow shock is formed in front of the vehicle due to supersonic flows. Pressure and temperature increases due to bow shock formation. Bow shock is tilted due to the free stream at an angle of 28 degrees.
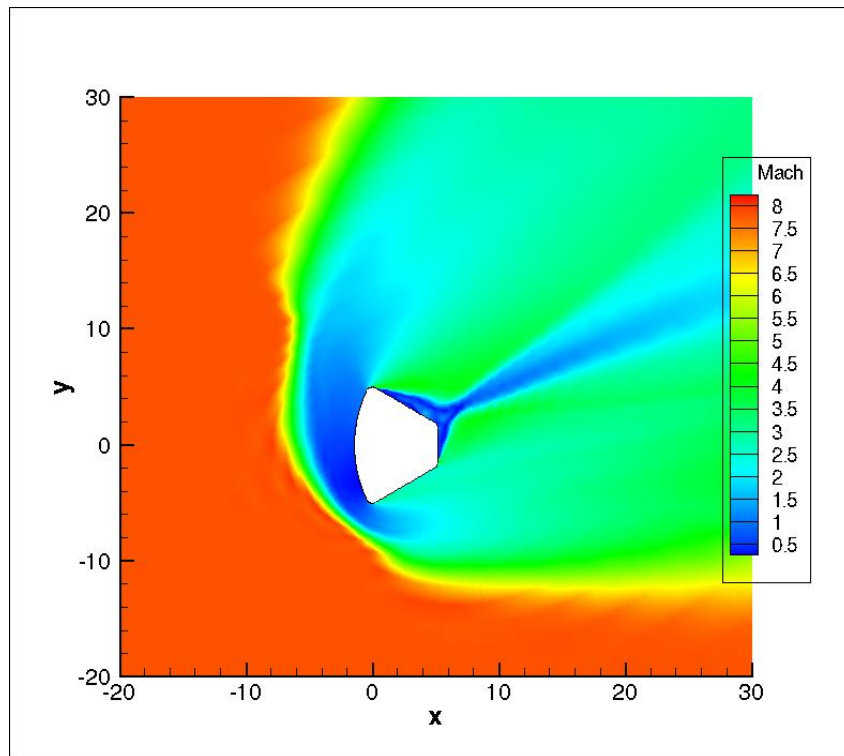
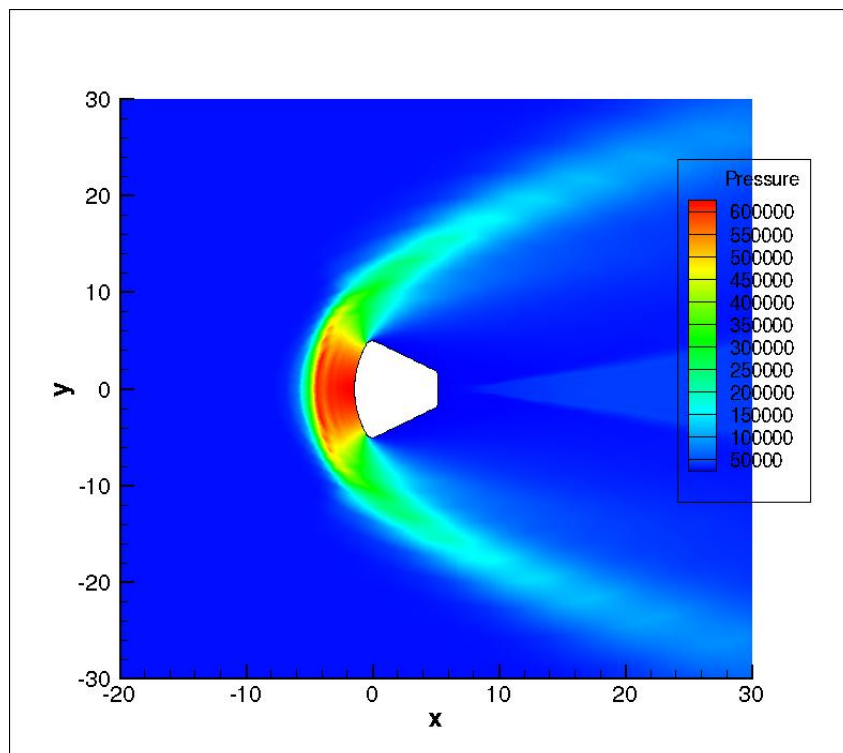Figure 3.2: Mach contours for mach 7.8 and 28^0 angle of attack
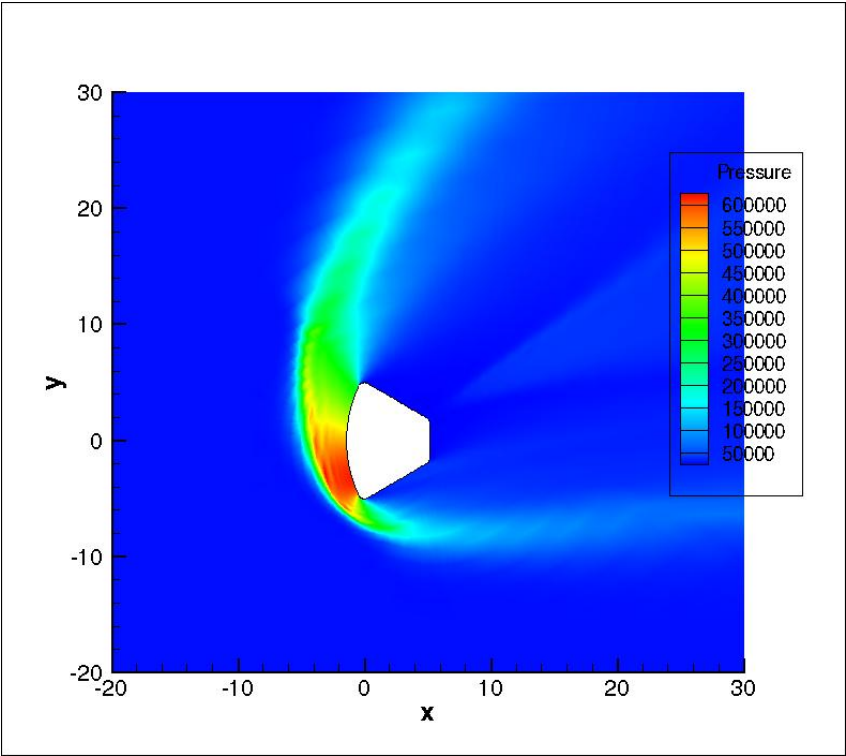
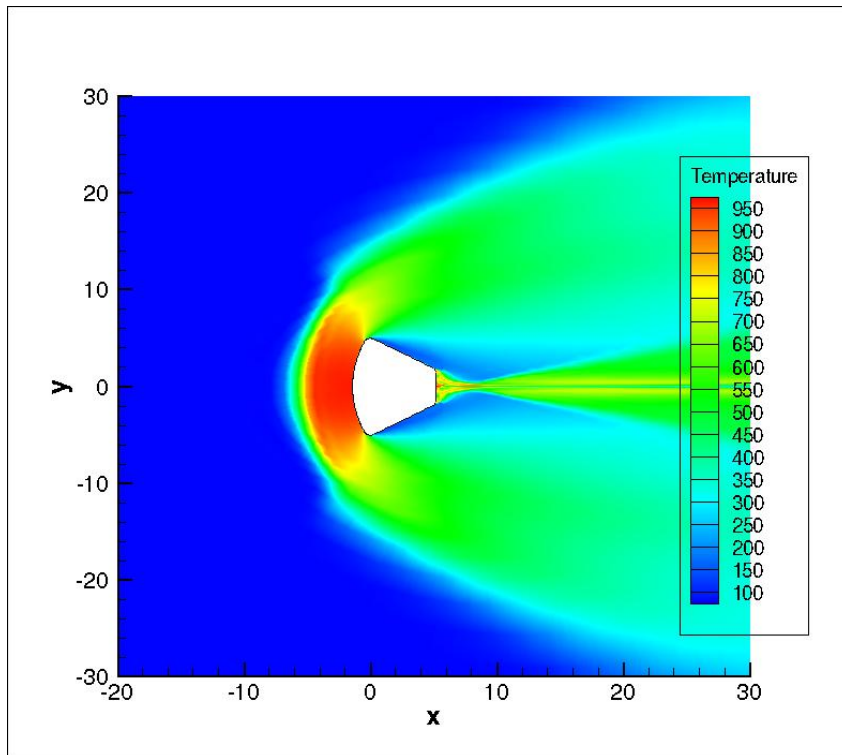Figure 3.3: Pressure contours for mach 7.8 and 28⁰ angle of attack
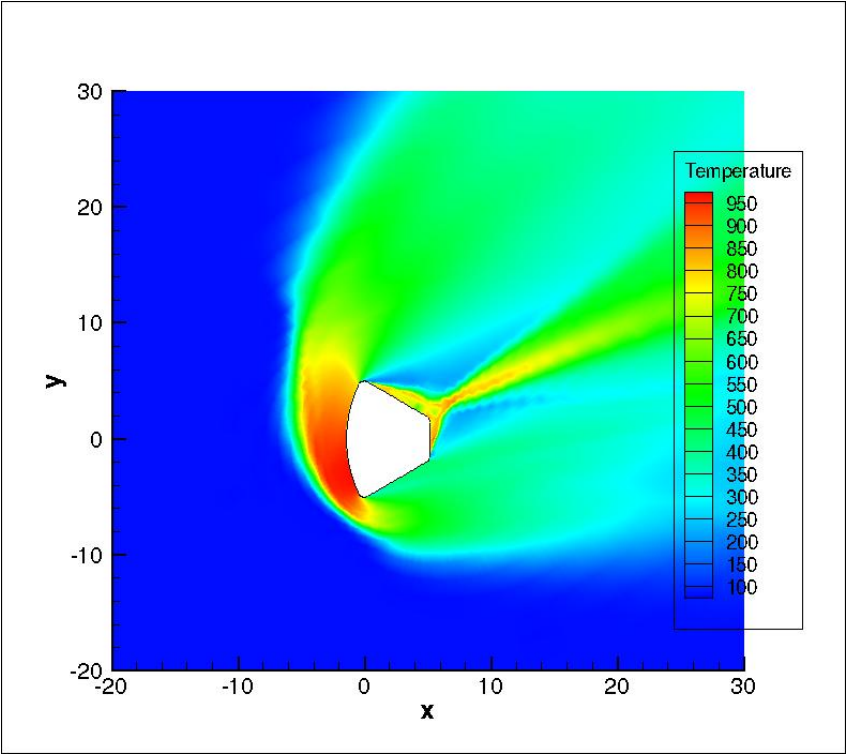
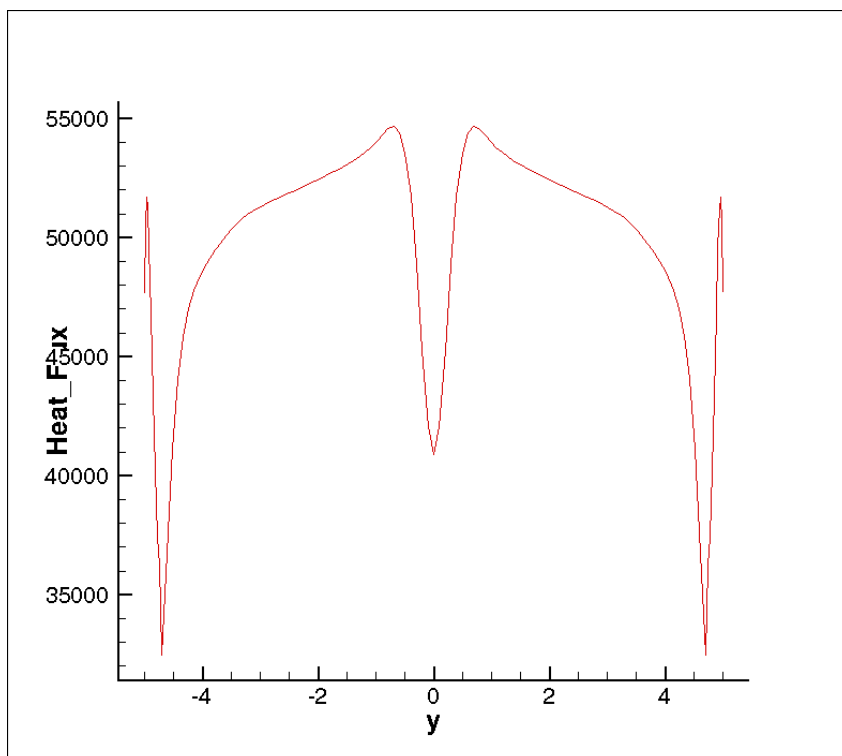Figure 3.4: Temperature contours for mach 7.8 and 28⁰ angle of attack
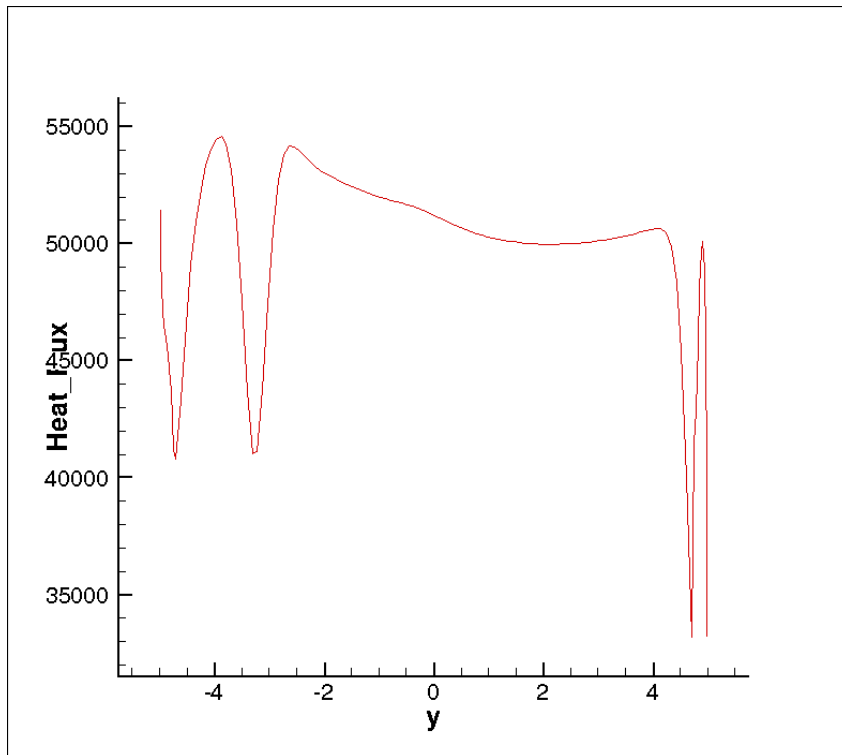
Figure 3.5: Heat Flux (W/m^2)distribution for mach 7.8 and 28^0 angle of attack along the surface
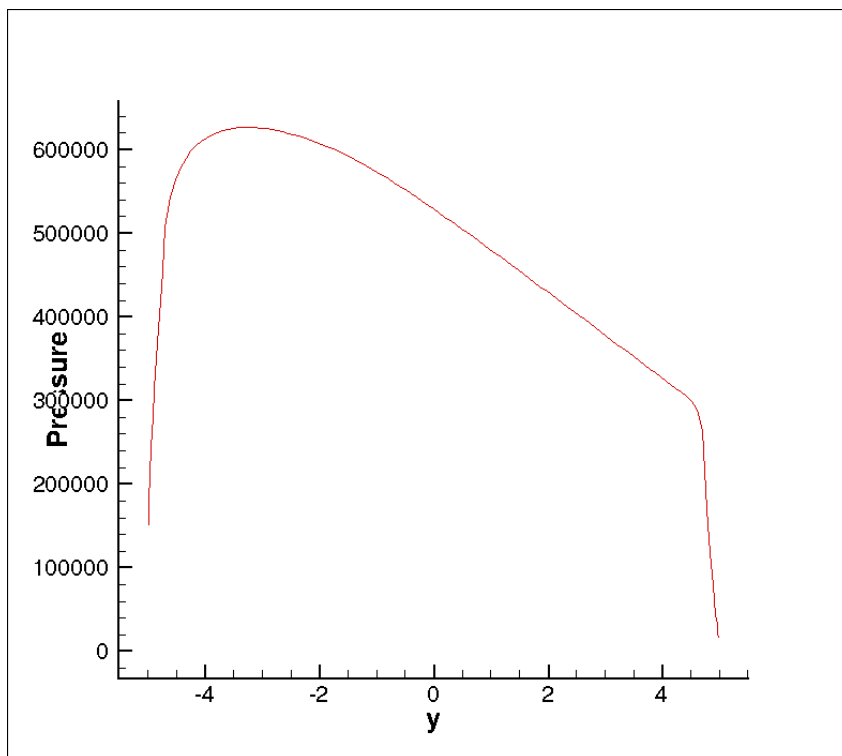
Figure 3.6: Pressure(Pa) distribution along the surface for mach 7.8 and 28^0 angle of attack

The stagnation point occurs at the point where the flow is incident to the surface. Since the angle of attack is 28 degree, the stagnation point is near to the sides. From Fig: 3.5, heat flux plot we can see that from the stagnation point the heat flux increases, this is because as the fluid moves from the center point to the sides through the radius, the boundary layer formed near to the surface will resist the flow of the fluid above it. So the kinetic energy of the fluid gets converted into the internal energy. As a result the temperature starts increasing and the heat flux also increases. After some point the interaction between the shock wave and boundary layer becomes less and the heat flux starts decreasing. After that there is expansion wave due to this temperature and heat flux decreases. Sudden raise of heat flux is due to meeting of shock and expansion waves. From Fig: 3.6 pressure plot we can see that the pressure is maximum at the stagnation region and it decreases to the sidewards.
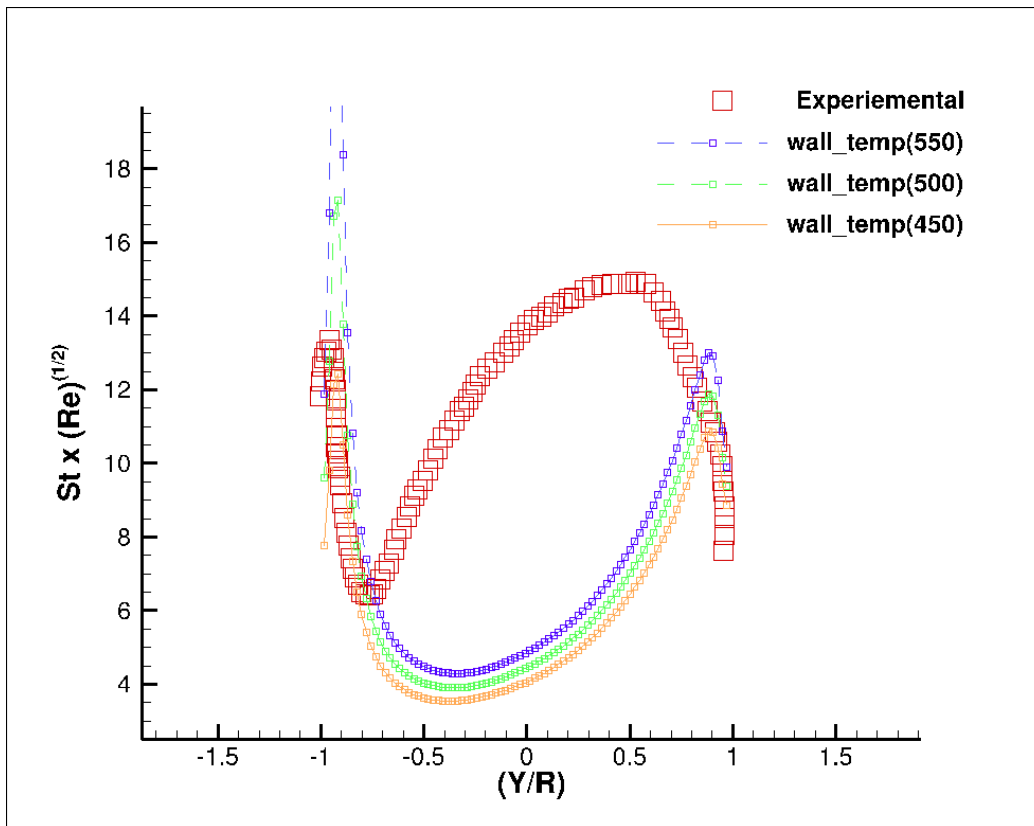
Figure 3.6: Comparison of experiemental data and the numerical results

The experimental data and the computational data are showing almost same trend. For wall temperature of 500, the experimental data is showing more similarity. At the corners the

computational data is showing good accuracy, but at the center there is a bit shifting of the values, this may be due to less computational accuracy.

3.3 Case Study

To know the flow field characteristics over a re-entry vehicle, first results are obtained for Mach number 7.8 at zero angle of attack. The operating conditions are given below.

Table 3.4: CEV test conditions

Reynolds number	10.072178E8
Mach	7.80
Angle of Attack	0.0
Pressure	8290 Pa
Temperature	74.1 K
Density	0.378 kg/m3
Velocity	1367 m/s

Mach, pressure and temperature contours are given for 0 degree angle of attack in Fig 3.7, 3.8 and 3.9. Since the angle of attack is 0 degree the stagnation point is at the center, so the pressure is maximum at this portion and it decreases along the radius.
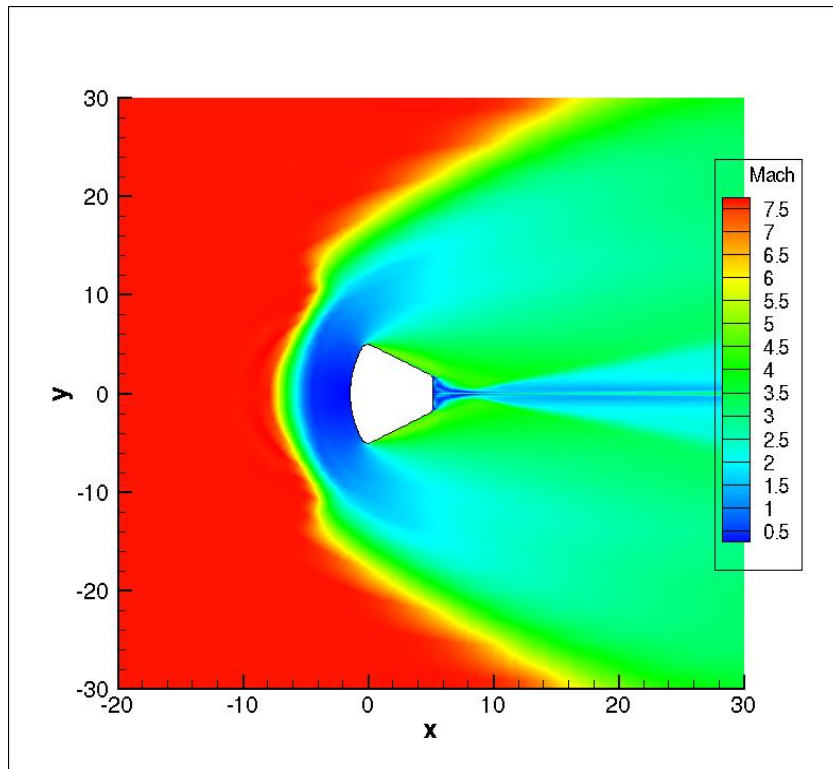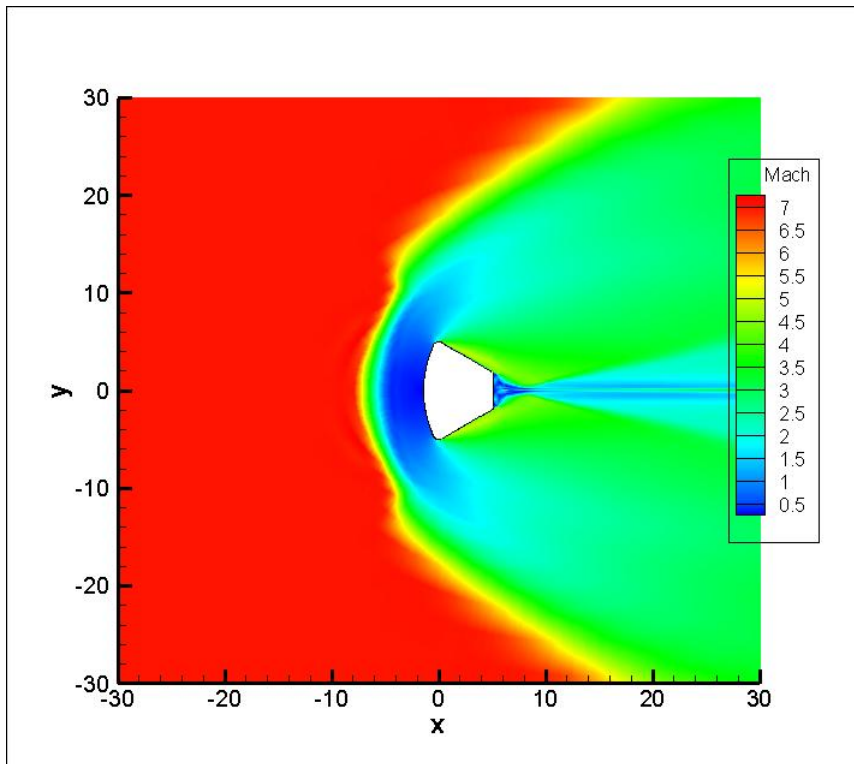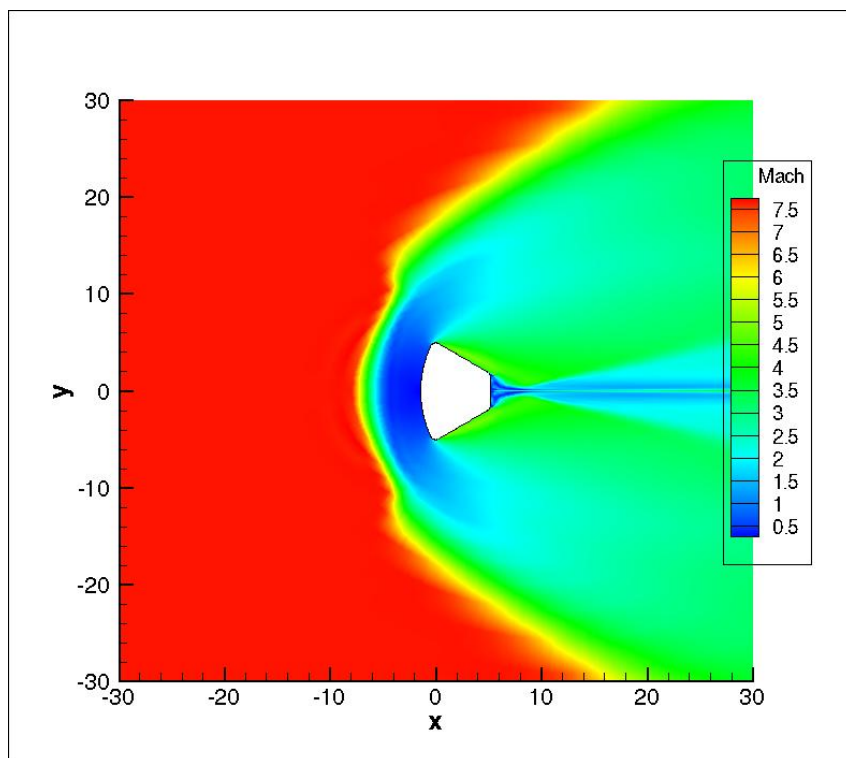
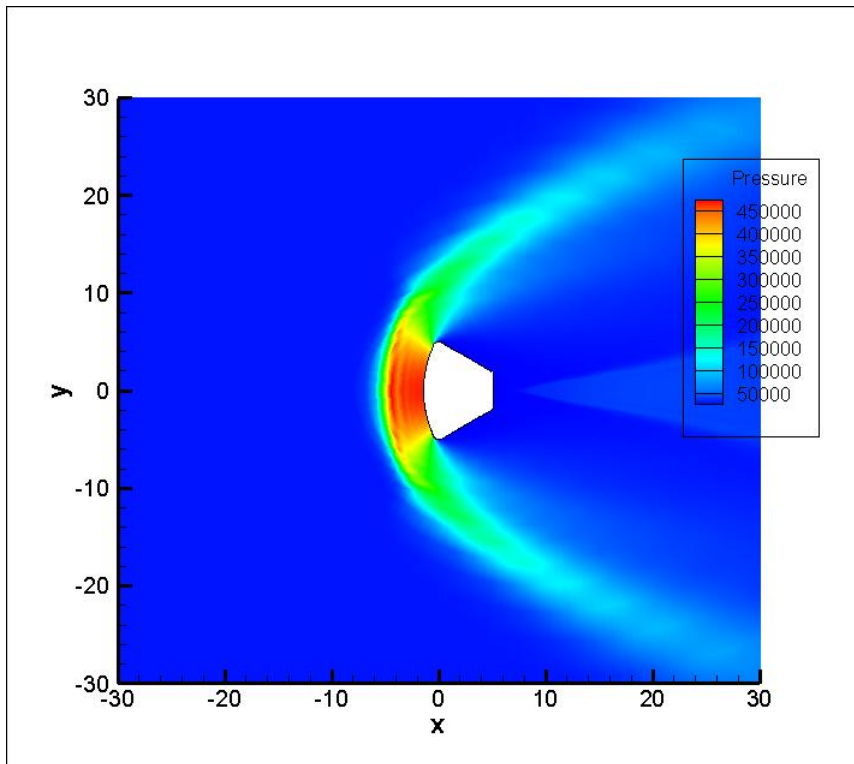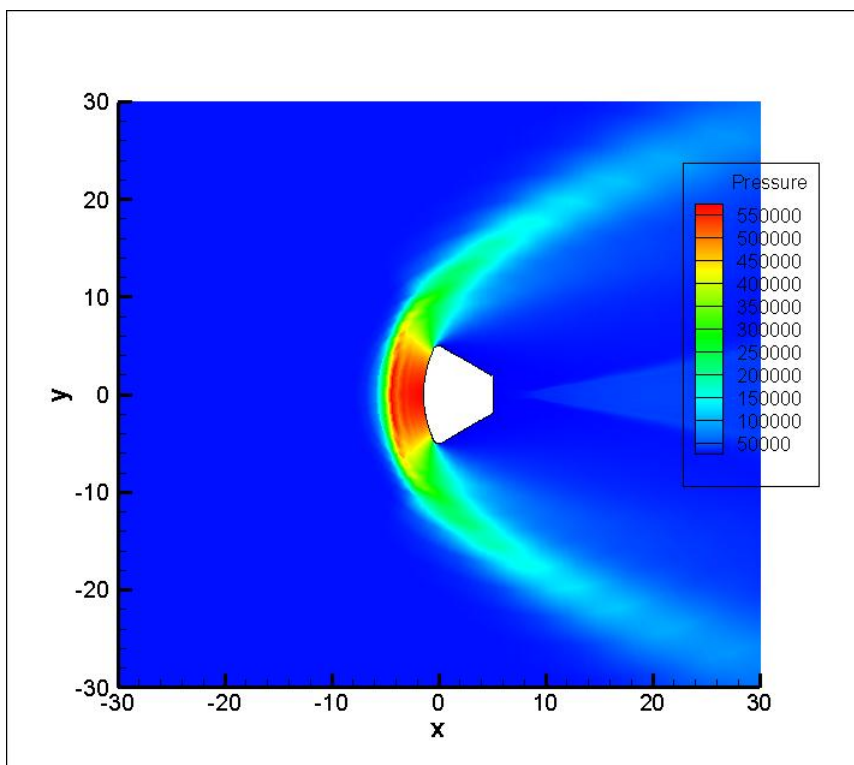Figure 3.7: Mach contours for mach 7.8 and 0^0 angle of attack

Figure 3.8: Pressure contours for mach 7.8 and 0^0 angle of attack

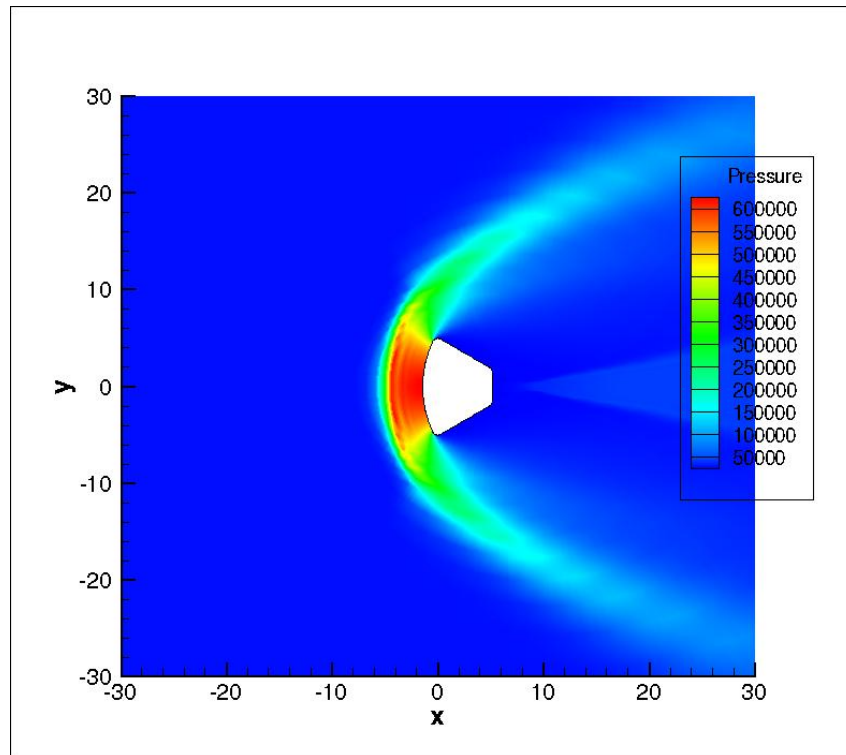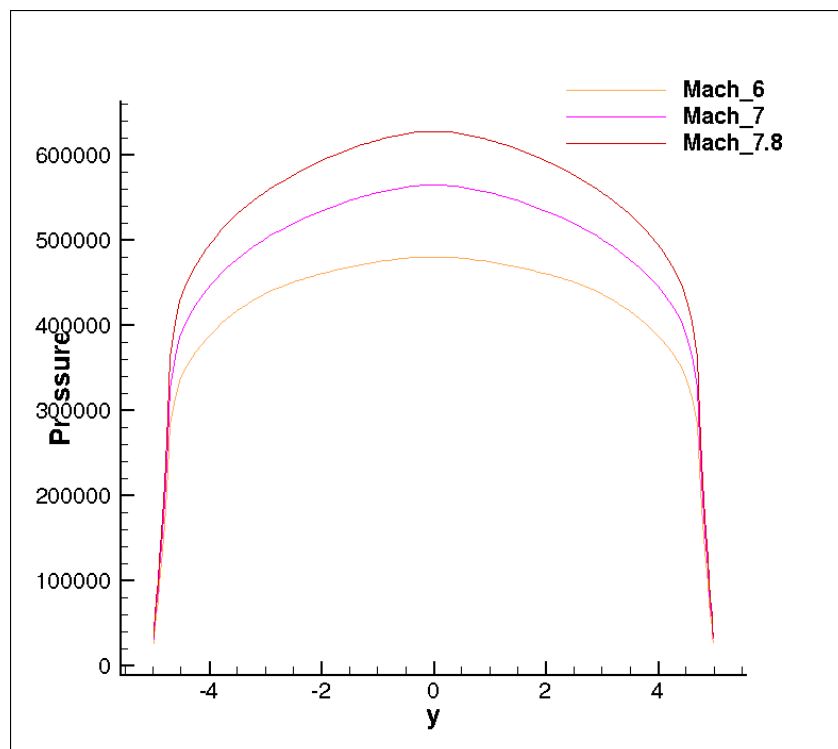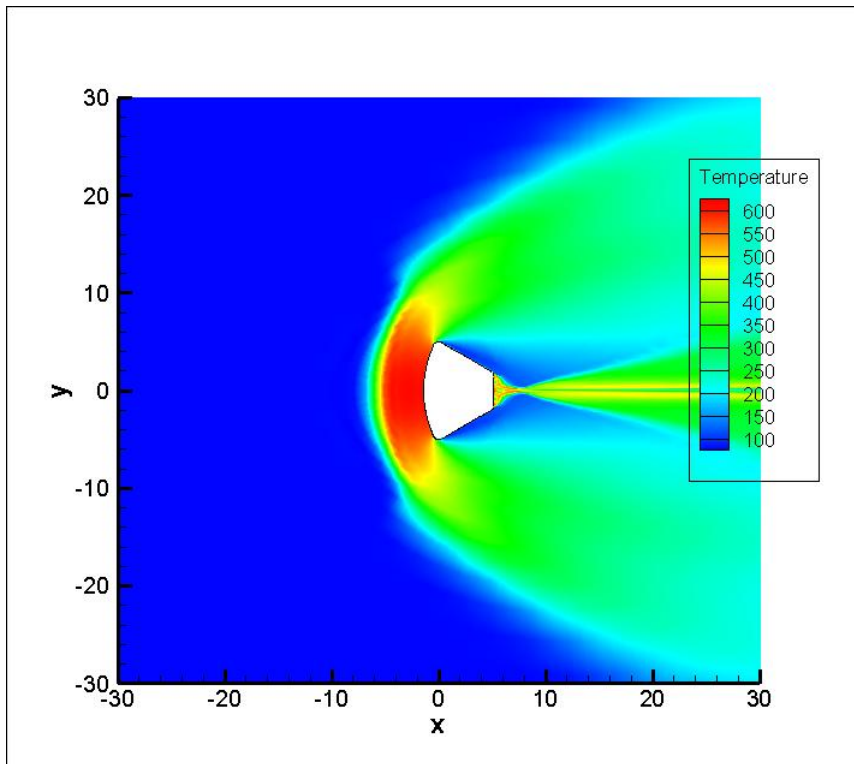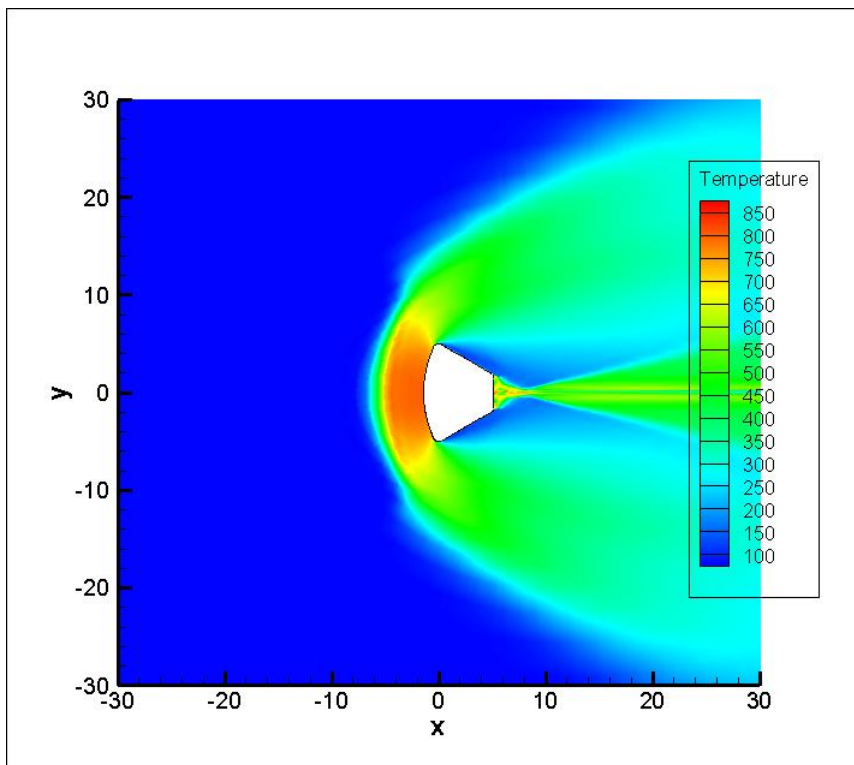Figure 3.9: Temperature contours for mach 7.8 and 0^0 angle of attack

Figure 3.10: Heat flux (W/m^2) distribution along the surface for mach 7.8 and 0^0 angle of attack
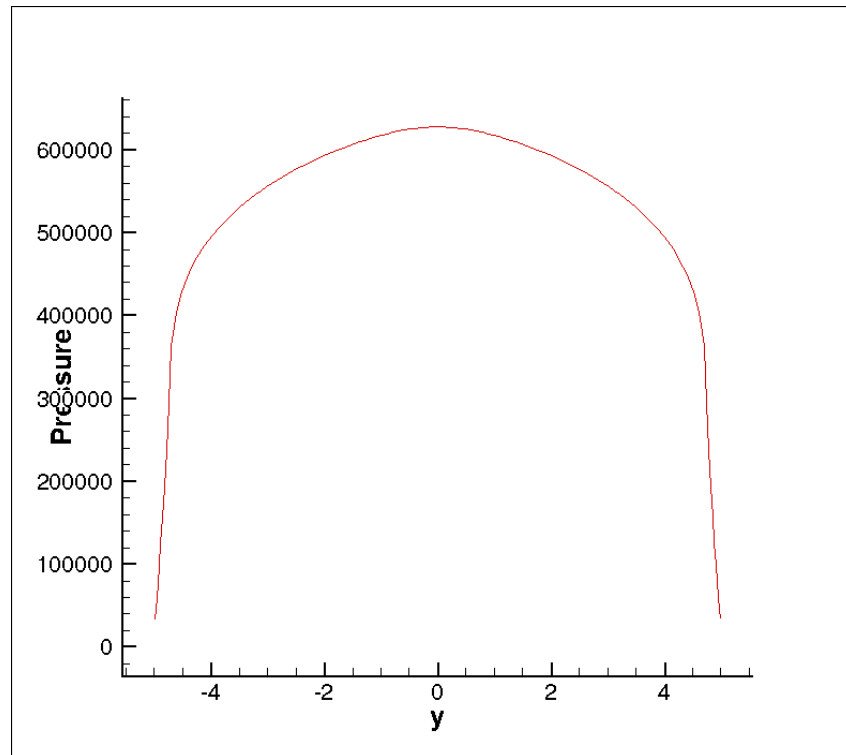
Figure 3.11: Pressure (Pa) distribution along the surface for mach 7.8 and 0^0 angle of attack

From the Mach, temperature and pressure contours we can see that a bow shock is formed in front of the re-entry vehicle. At the corners of the re-entry vehicle the bow shock get detached and the expansion wave begins. At the centre of the re-entry vehicle is the stagnation point, the fluid will be at rest in this point and the pressure here is the stagnation pressure and the temperature here is the stagnation temperature. From heat flux plot we can see that from the stagnation point the heat flux increases, this is because as the fluid moves from the center point to the sides through the radius, the boundary layer formed near to the surface will resist the flow of the fluid above it. So the kinetic energy of the fluid gets converted into the internal energy. As a result the temperature starts increasing and the heat flux also increases. After some point the interaction between the shock wave and boundary layer becomes less and the heat flux starts decreasing. After that there is expansion wave due to this temperature and heat flux decreases. Sudden raise of heat flux is due to meeting of shock and expansion waves. From pressure plot we can see that the pressure is maximum at the stagnation region and it decreases to the sidewards.

3.4 Effect of Different Mach Number

To know the change in flow field characteristics over re-entry vehicle with the change in the Mach number at an angle of attack of zero. The operating conditions are given below:

Table 3.5: CEV test conditions for different Mach numbers

Reynolds number	10.072178E8
Angle of attack	0
Pressure	8290 Pa
Temperature	74.1 K
Density	0.378 kg/m3
Velocity	1367 m/s
Wall Temperature	394 K
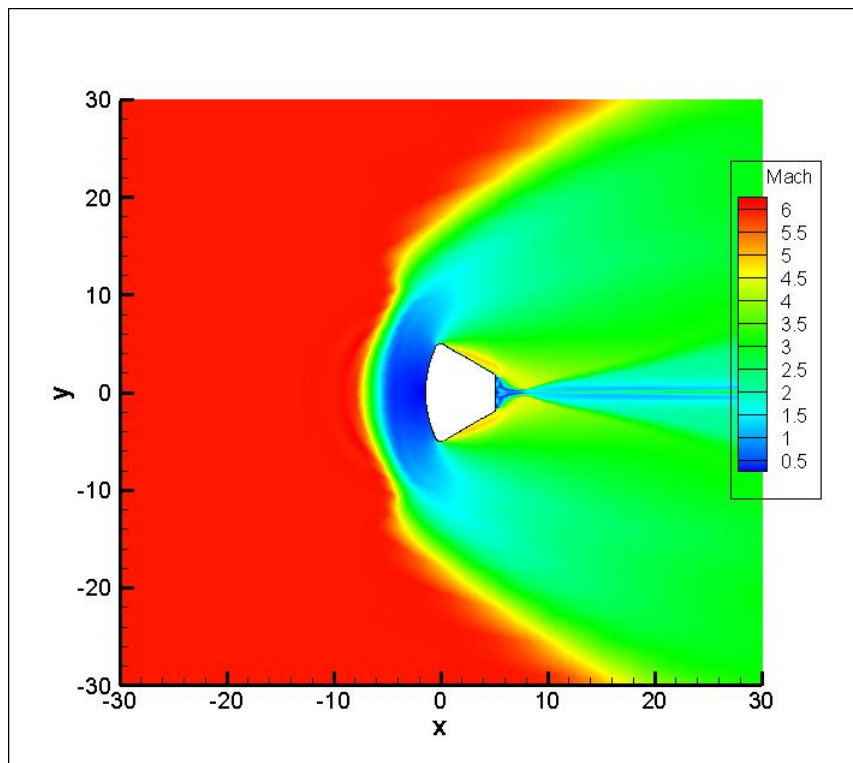
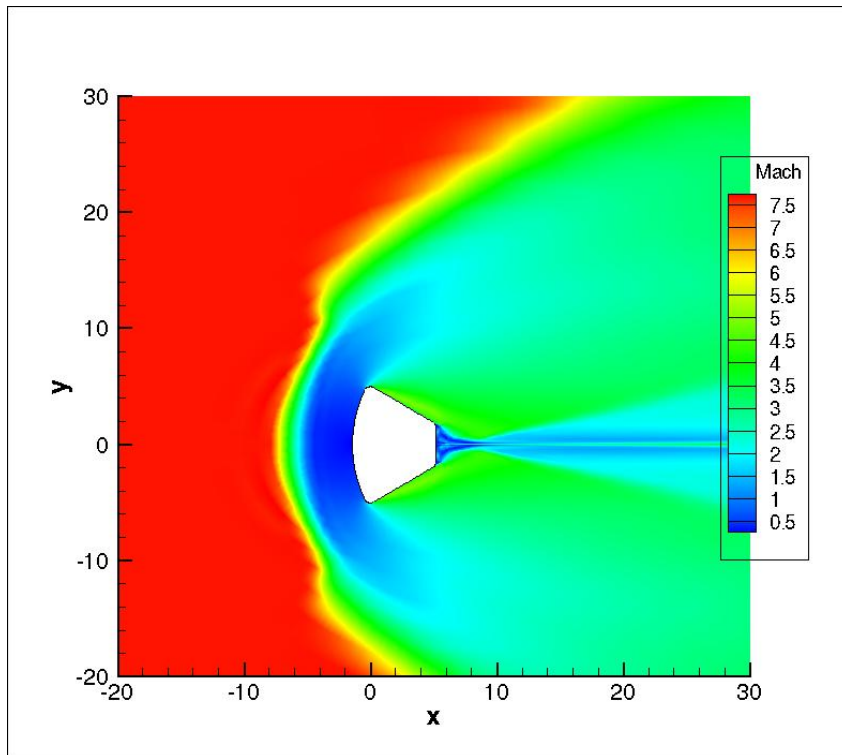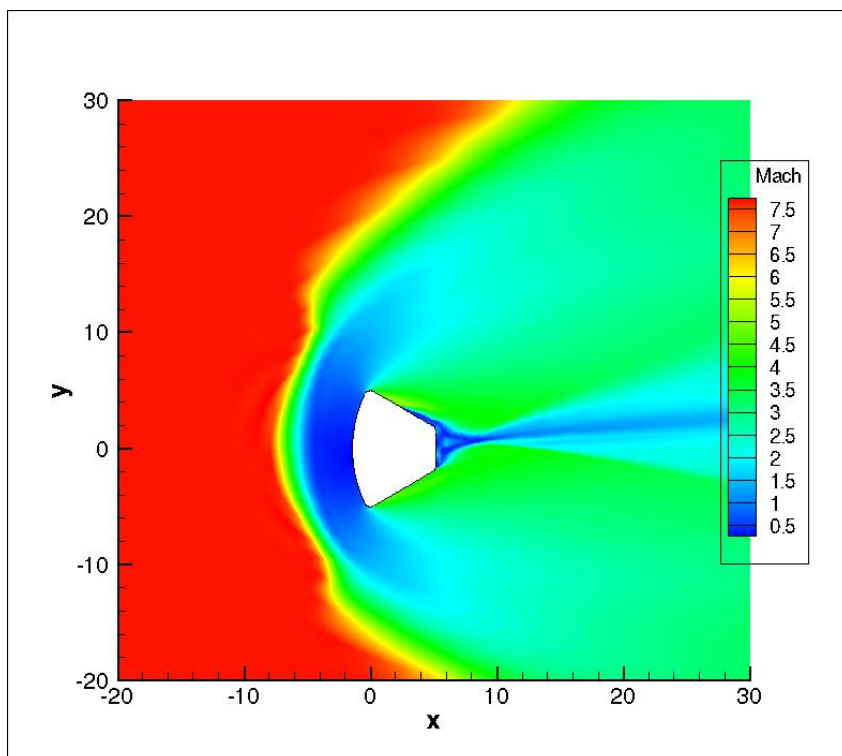Figure 3.12: Mach contours for mach 6.0 and 0^0 angle of attack
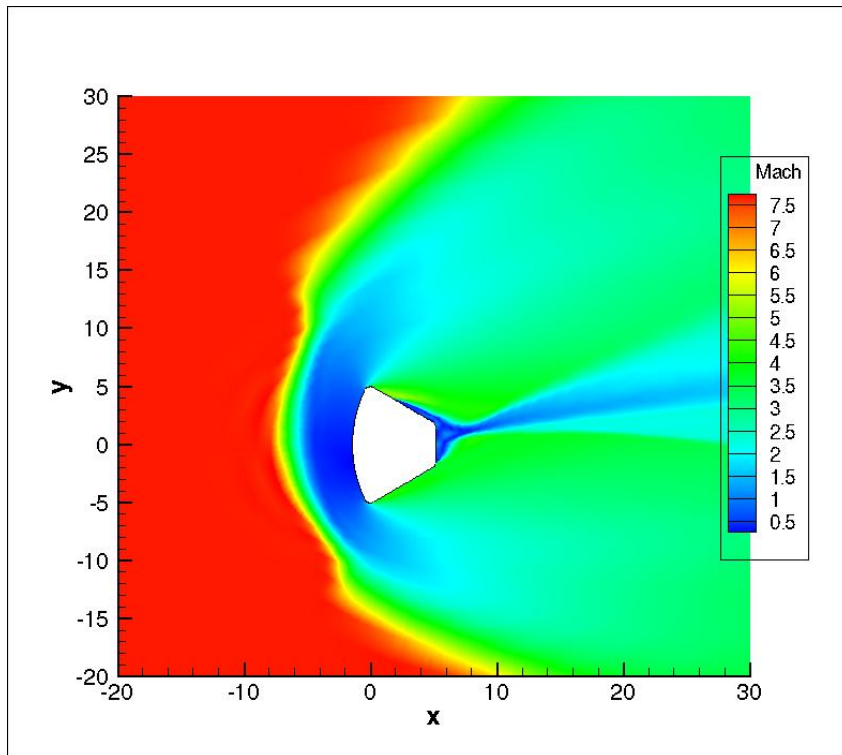
Figure 3.13: Mach contours for mach 7.0 and 0^0 angle of attack

Figure 3.14: Mach contours for mach 7.8 and 0^0 angle of attack

28

Figure 3.15: Pressure contours for mach 6.0 and 0^0 angle of attack

Figure 3.16: Pressure contours for mach 7.0 and 0^0 angle of attack

Figure 3.17: Pressure contours for mach 7.8 and 0^0 angle of attack

Figure 3.18: Comparison of pressure surface value for different mach number

Figure 3.19: Temperature contours for mach 6.0 and 0^0 angle of attack

Figure 3.20: Temperature contours for mach 7.0 and 0^0 angle of attack
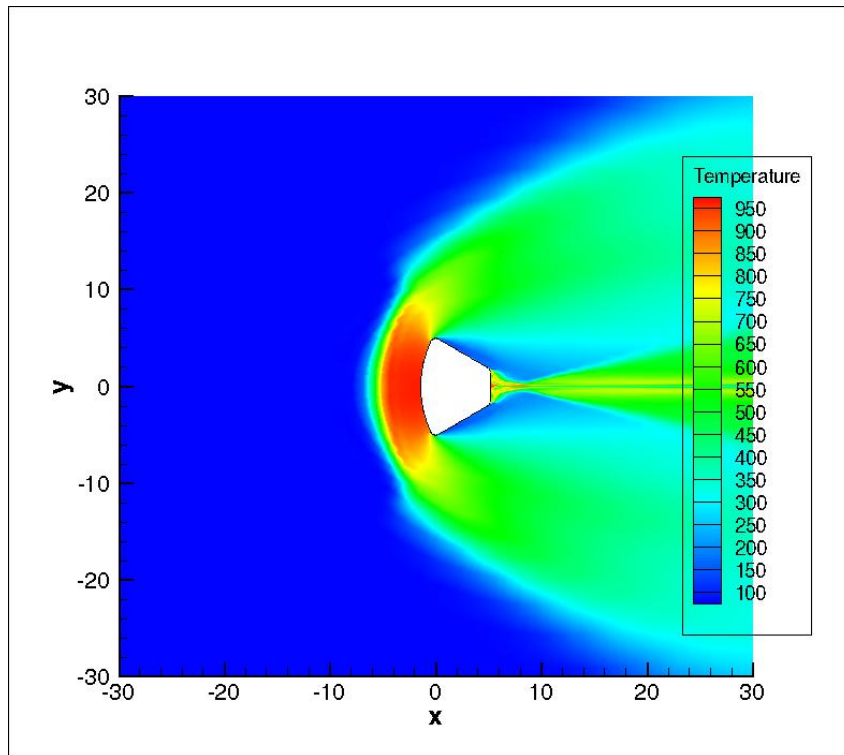
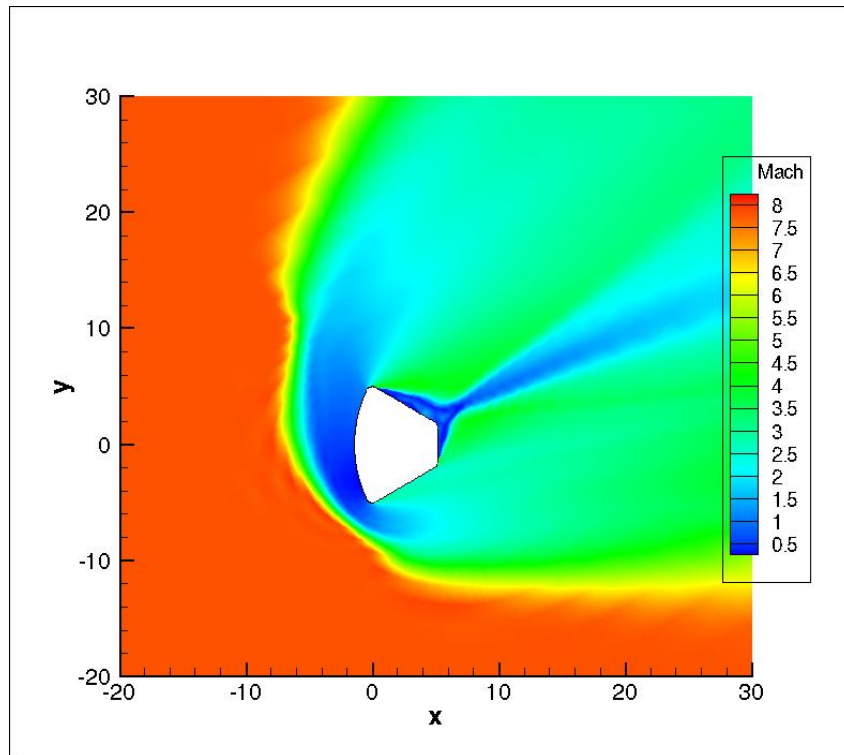Figure 3.21: Temperature contours for mach 7.8 and 0^0 angle of attack
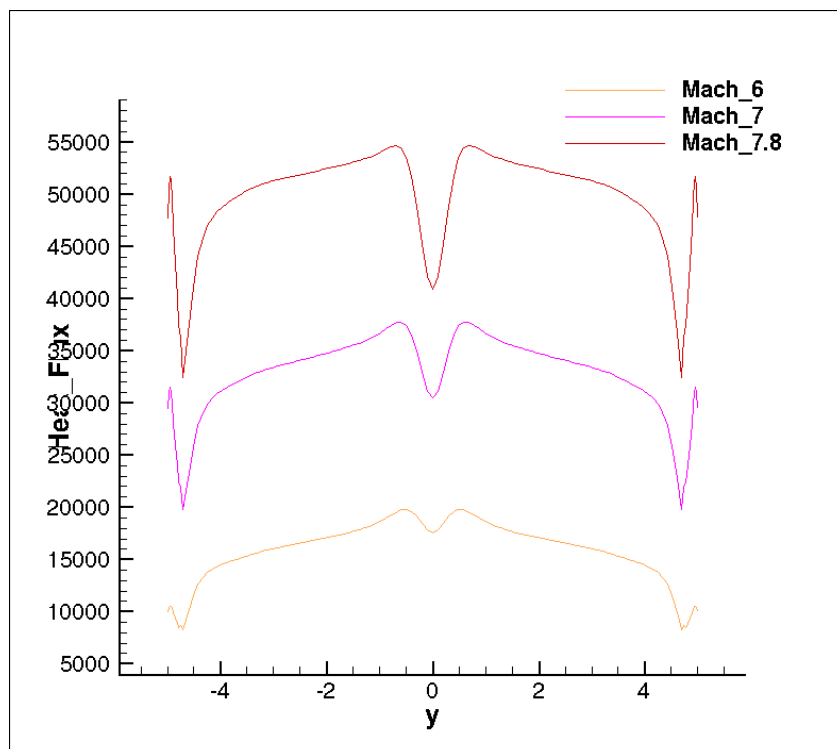
Figure 3.22: Comparison of heat flux surface value for different mach number

Table 3.6: Shock distance for different mach number

Mach Number	Shock Distance (m)
6	2.99102
7	2.98805
7.8	2.98325

From the mach, pressure and temperature contours we can see that as we increase the Mach number, the bow shock strength increases and the temperature also get increased. In Table 3.6, the bow shock distance for different mach numbers are given, from this table it is clear that as we increase the Mach number the shock distance comes closer to the body. Heat flux also increases with increase in the Mach number.

3.5 Effect of different angle of attacks

To know the change in flow characteristics of re-entry vehicle at Mach number of 7.8 with change in angle of attacks. The operating conditions are given below:

Table 3.7: CEV test conditions for different angle of attacks

Reynolds number	10.072178E8
Mach number	7.80
Pressure	8290 Pa
Temperature	74.1 K
Density	0.378 kg/m3
Velocity	1367 m/s
Wall Temperature	394 K

Figure 3.23: Mach contours for mach 7.8 and 0^0 angle of attack

Figure 3.24: Mach contours for mach 7.8 and 5^0 angle of attack

Figure 3.25: Mach contours for mach 7.8 and 10^0 angle of attack
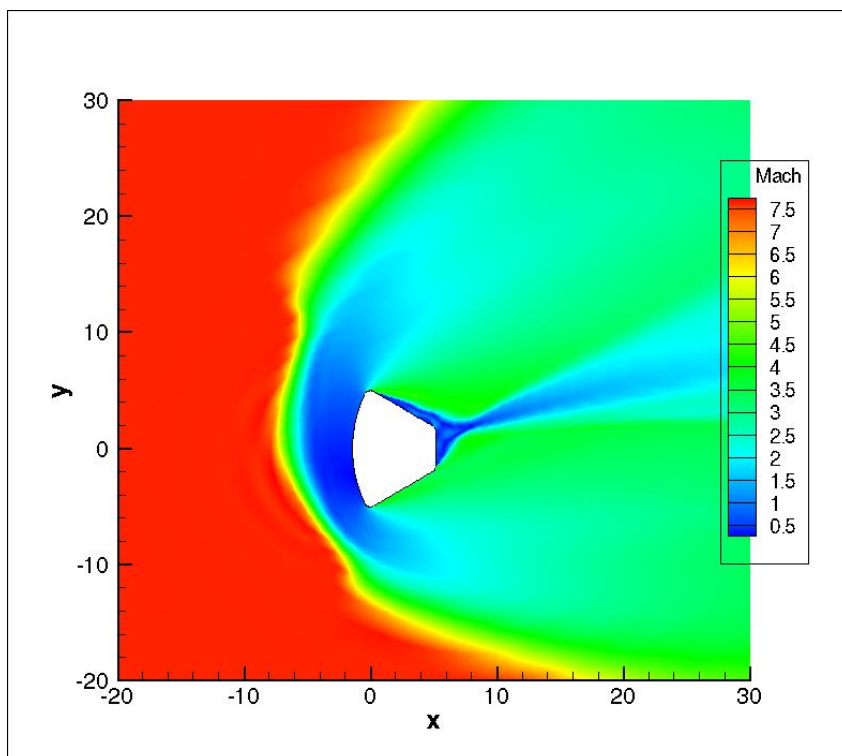
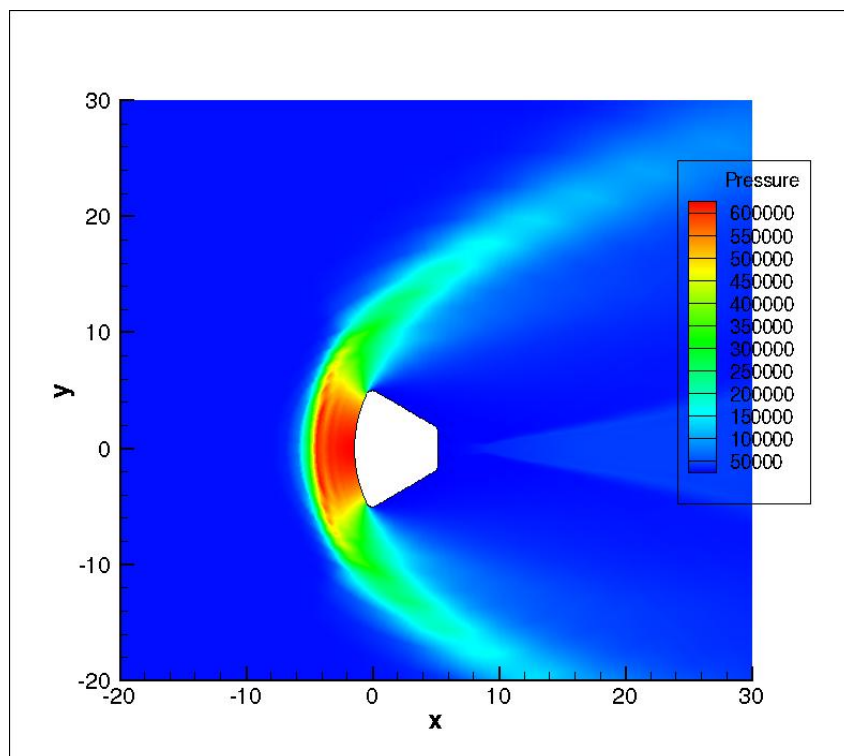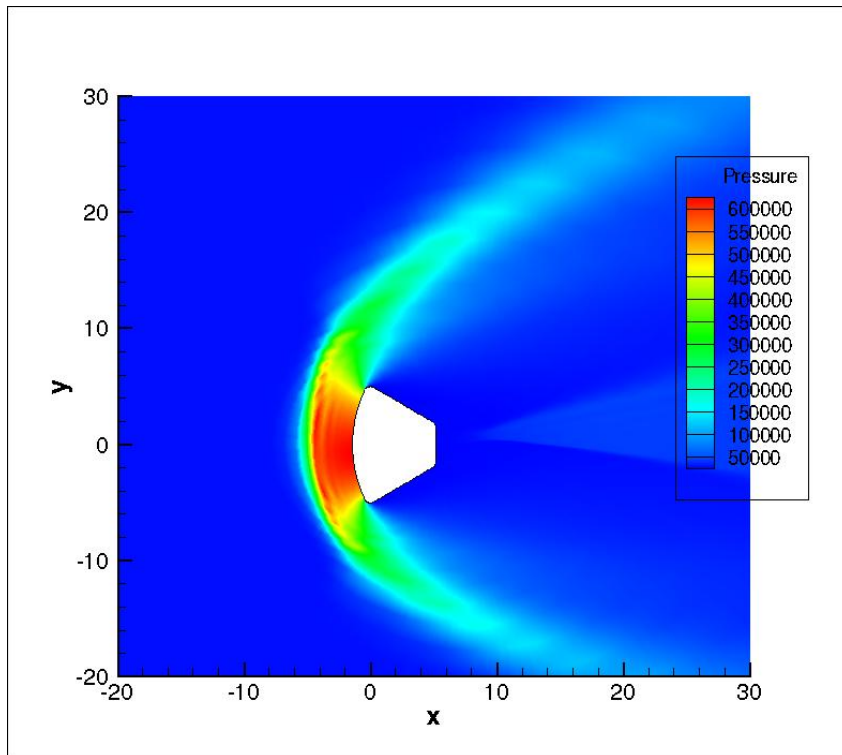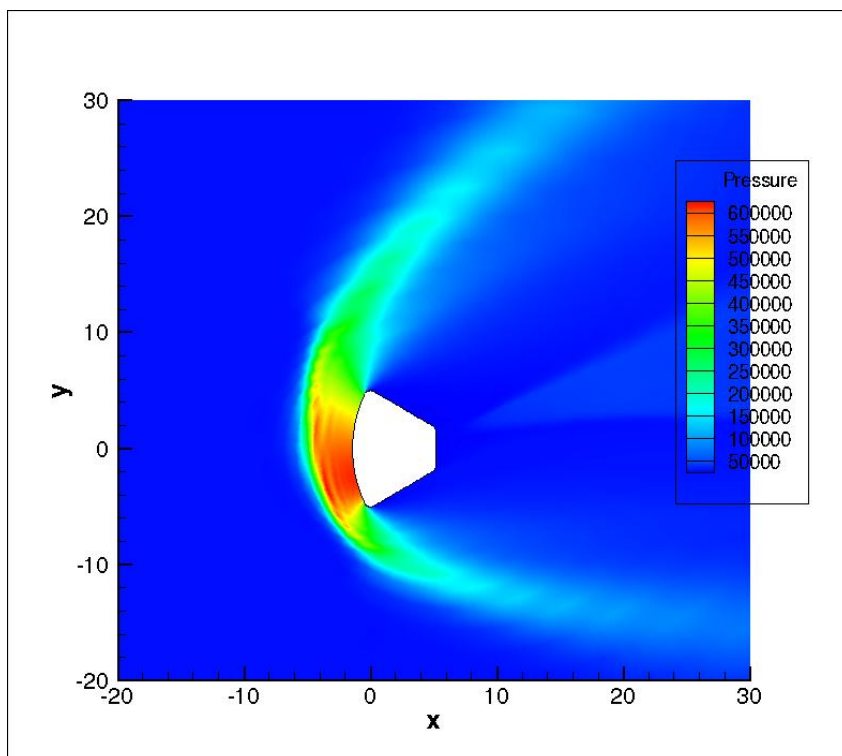Figure 3.26: Mach contours for mach 7.8 and 15^0 angle of attack
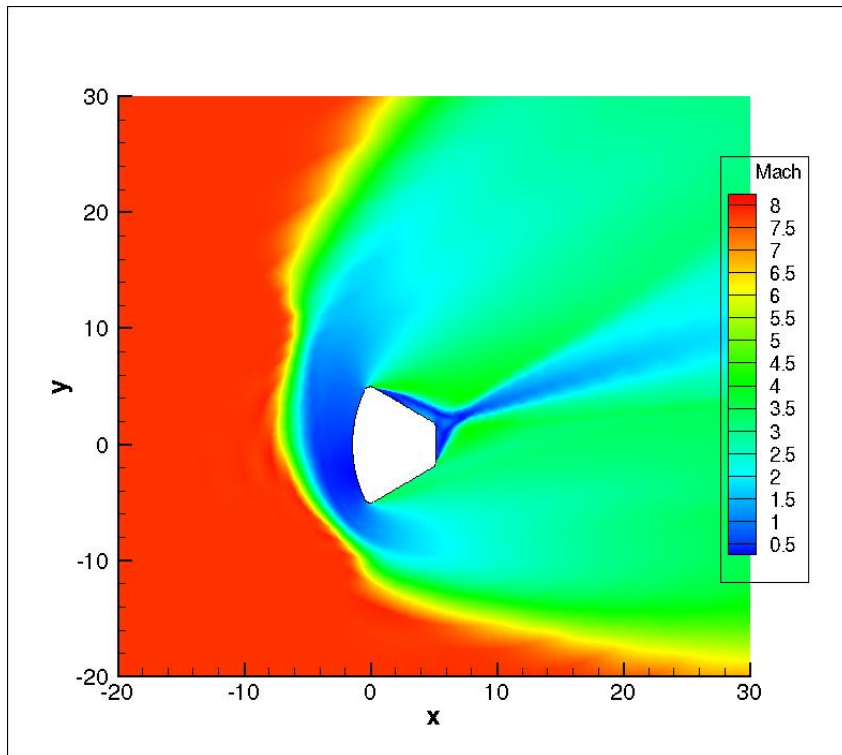
Figure 3.27: Mach contours for mach 7.8 and 20^0 angle of attack
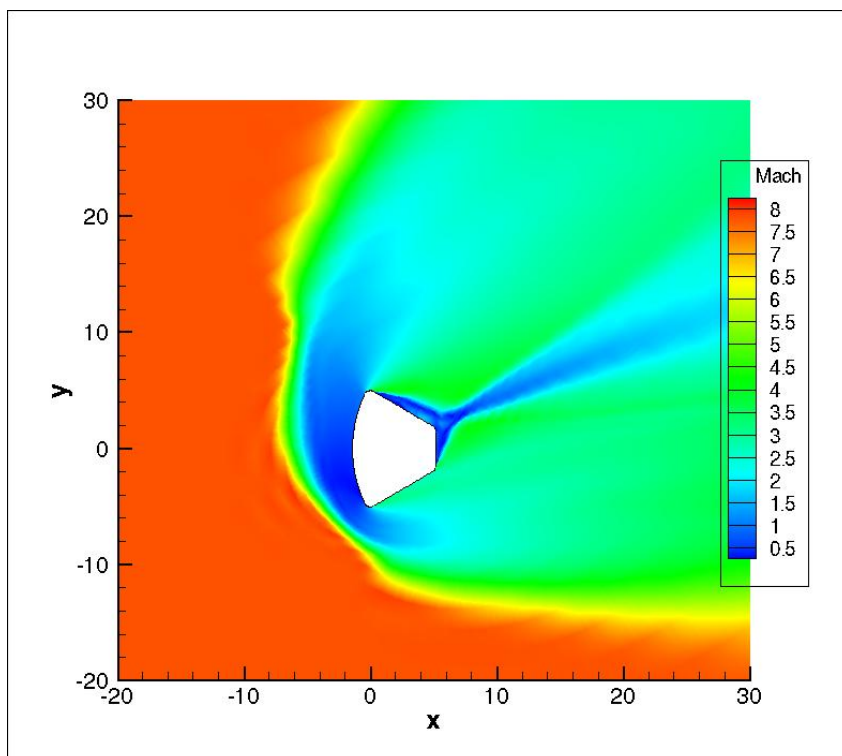
Figure 3.28: Mach contours for mach 7.8 and 25^0 angle of attack

Figure 3.29: Mach contours for mach 7.8 and 28⁰ angle of attack

Figure 3.30: Pressure contours for mach 7.8 and 0⁰ angle of attack

Figure 3.31: Pressure contours for mach 7.8 and 5^0 angle of attack

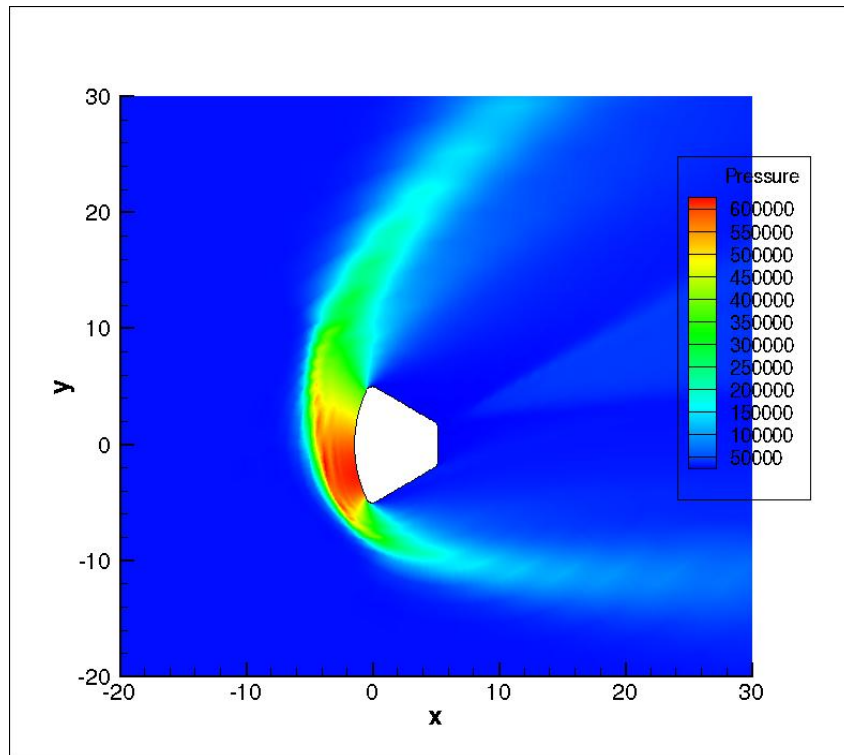Figure 3.32: Pressure contours for mach 7.8 and 10^0 angle of attack

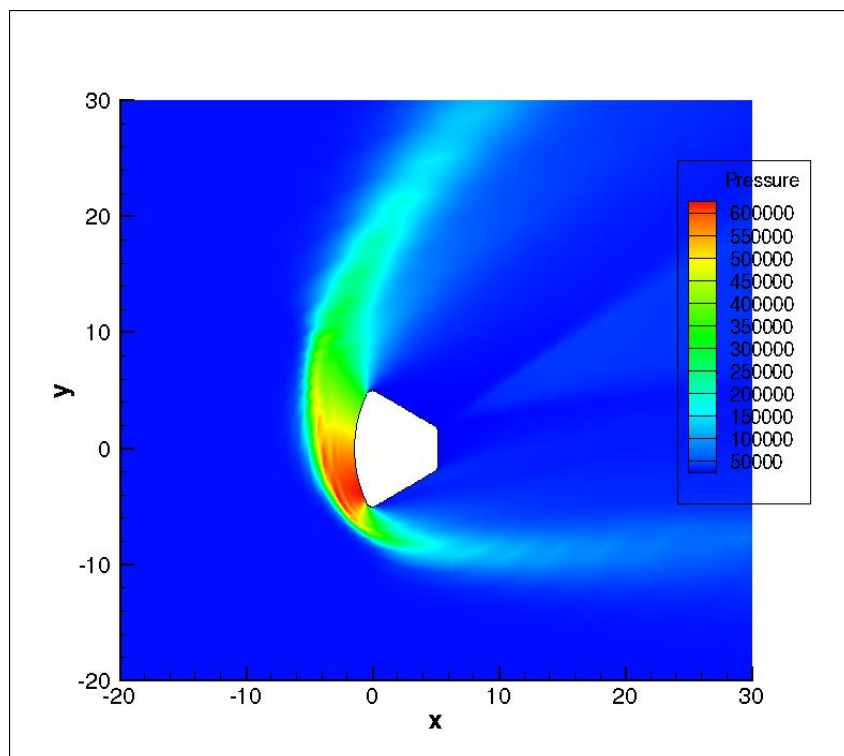Figure 3.33: Pressue contours for mach 7.8 and 15^0 angle of attack

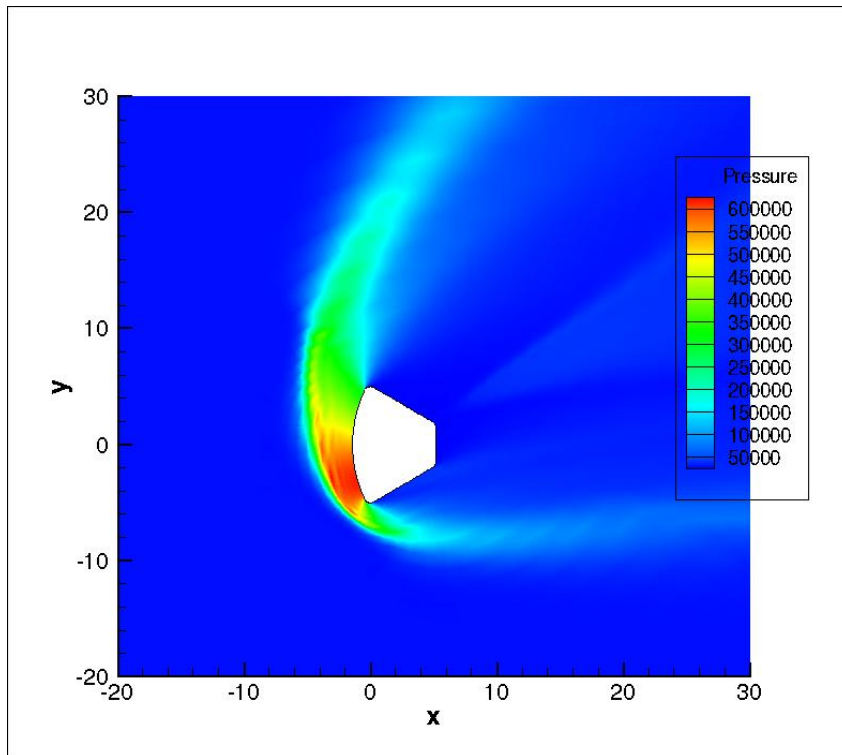Figure 3.34: Pressure contours for mach 7.8 and 20^0 angle of attack

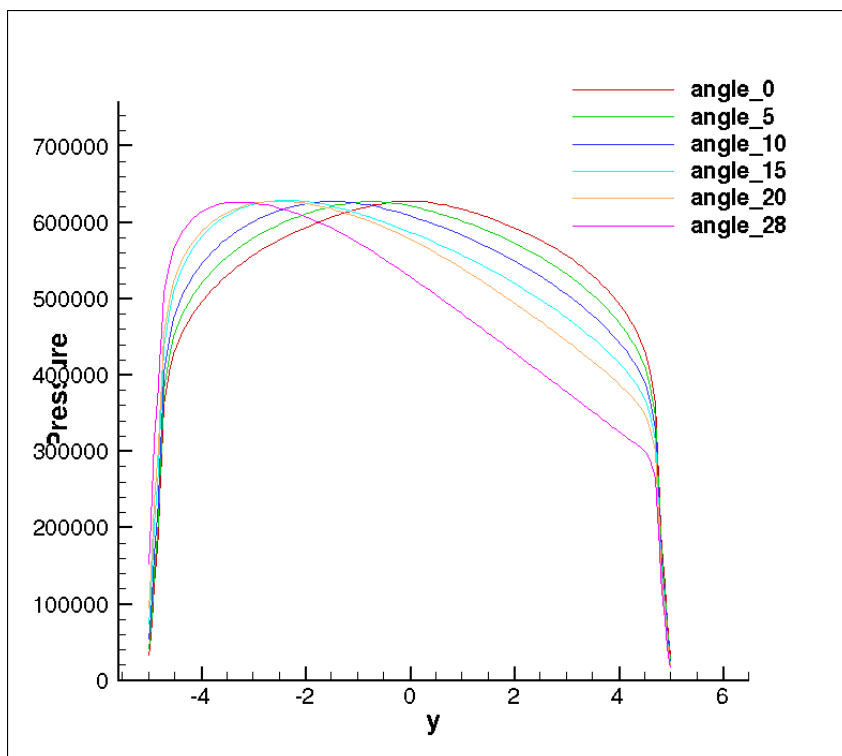Figure 3.35: Pressure contours for mach 7.8 and 28^0 angle of attack

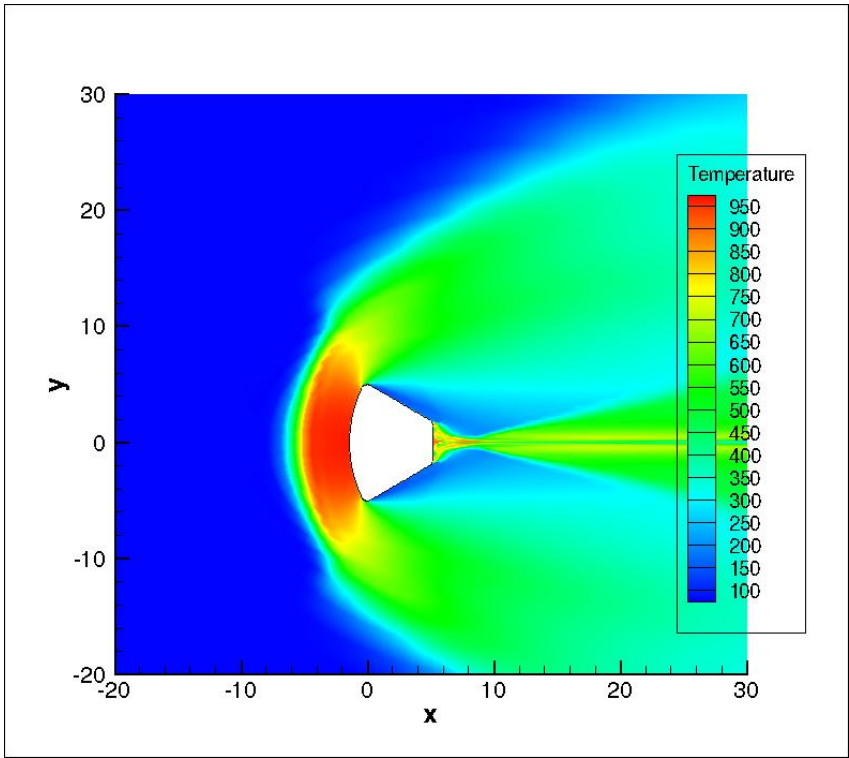Figure 3.36: Comparison of Pressure (Pa) for different angle of attack.

Figure 3.37: Temperature contours for mach 7.8 and 0^0 angle of attack
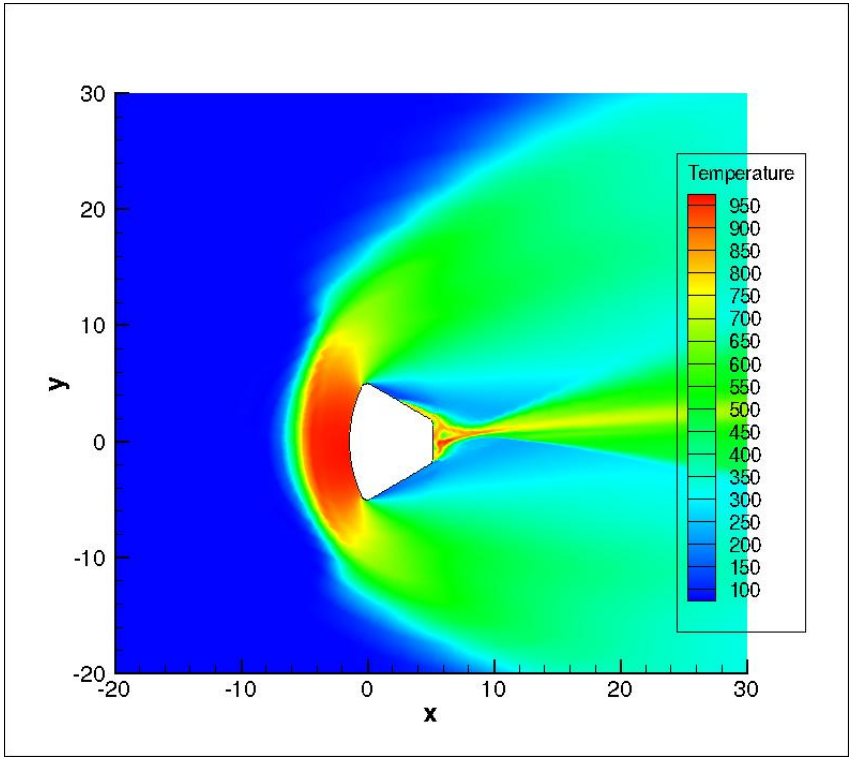

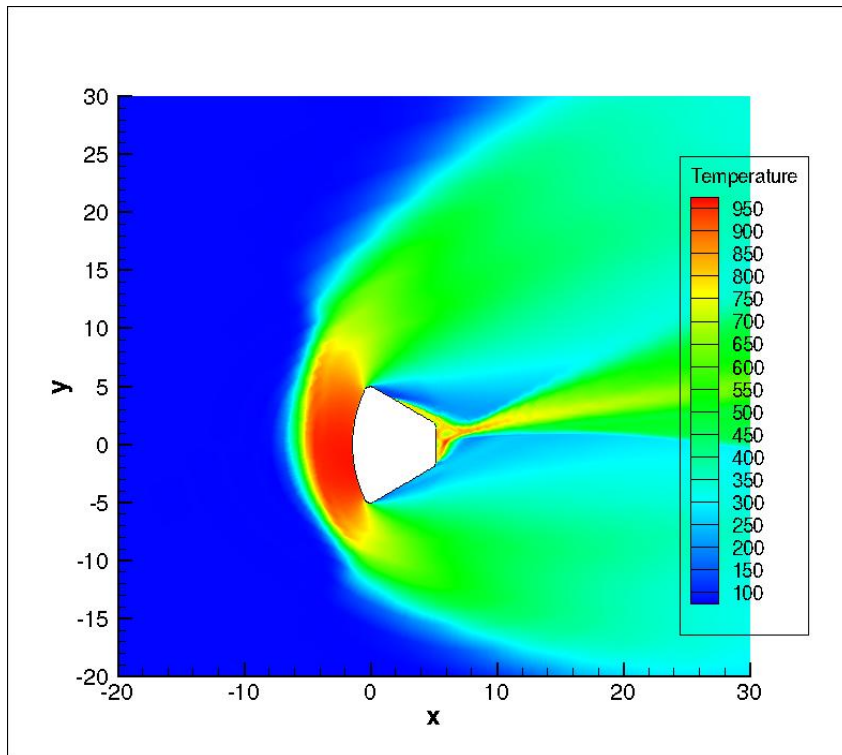Figure 3.38: Temperature contours for mach 7.8 and 5^0 angle of attack

Figure 3.39: Temperature contours for mach 7.8 and 10^0 angle of attack

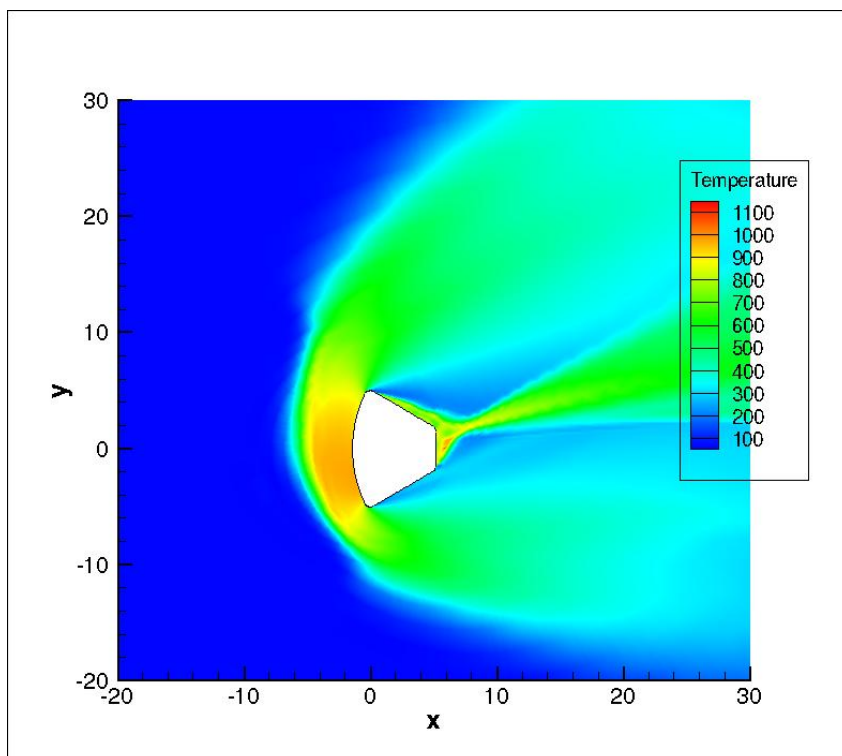

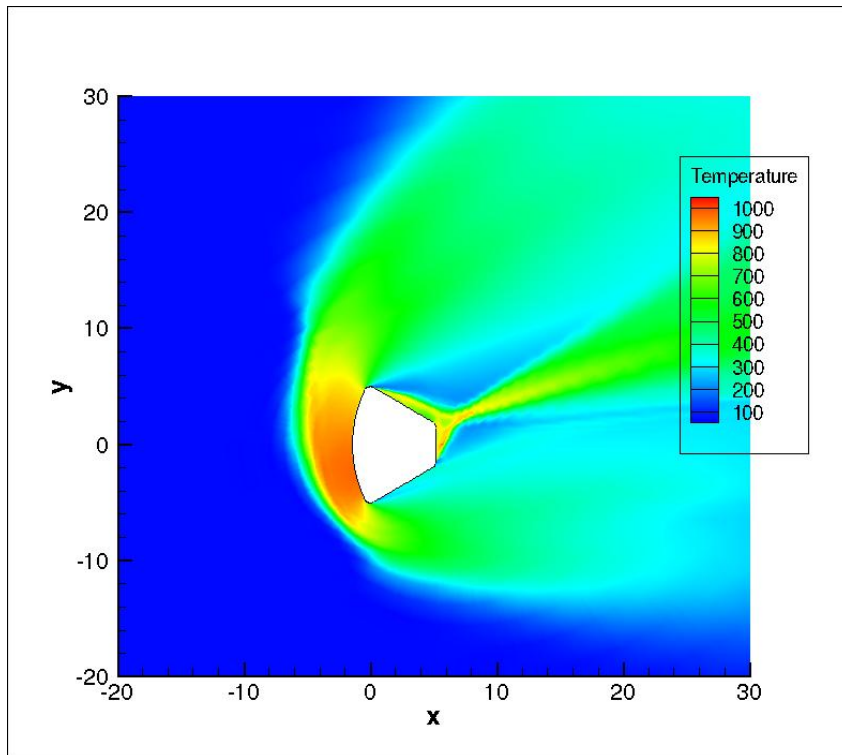Figure 3.40: Mach contours for mach 7.8 and 15^0 angle of attack

Figure 3.41: Temperature contours for mach 7.8 and 20^0 angle of attack
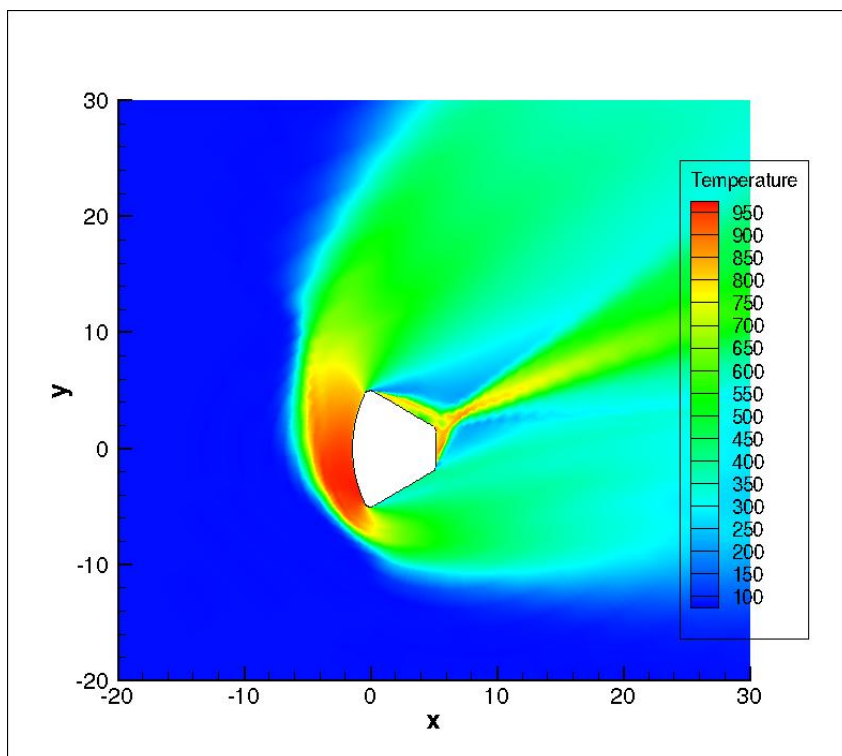

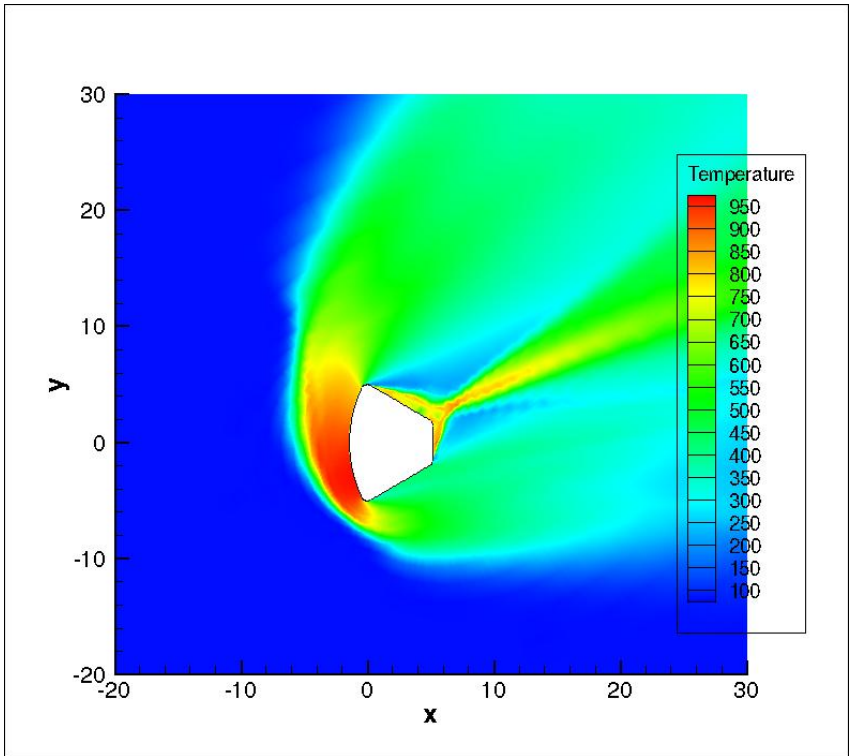Figure 3.42: Temperature contours for mach 7.8 and 25^0 angle of attack

Figure 3.43: Temperature contours for mach 7.8 and 28^0 angle of attack
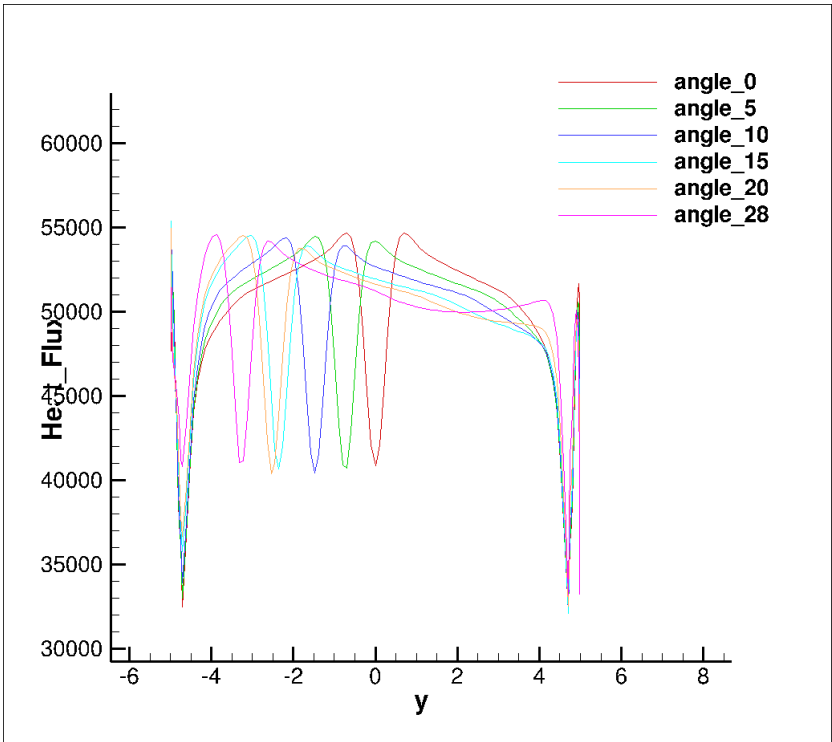
Figure 3.44: Comparison of heat flux (W/m²) for different angle of attack for mach number 7.80

45

Here we can see that there is no much difference in the stagnation temperature and stagnation pressur with the change in the angle of attack. But the stagnation point will change according to the change in the angle of attack. The maximum pressure and peak surface heat flux location shifts from the center to bottom side with increase in angle of attack from 0 degrees to 28 degrees.

3.6 Effect of different wall temperatures

To know the change in flow characteristics of re-entry vehicle at Mach number of 7.8 with change in angle of attacks. The operating conditions are given below:

Table 3.8: CEV test conditions for different wall temperatures

Reynolds number	10.072178E8
Angle of attack	0
Mach number	7.80
Pressure	8290 Pa
Temperature	74.1 K
Density	0.378 kg/m3
Velocity	1367 m/s

Figure 3.45: Comparison of heat flux for different wall temperature for mach number 7.80 and angle of attack 0
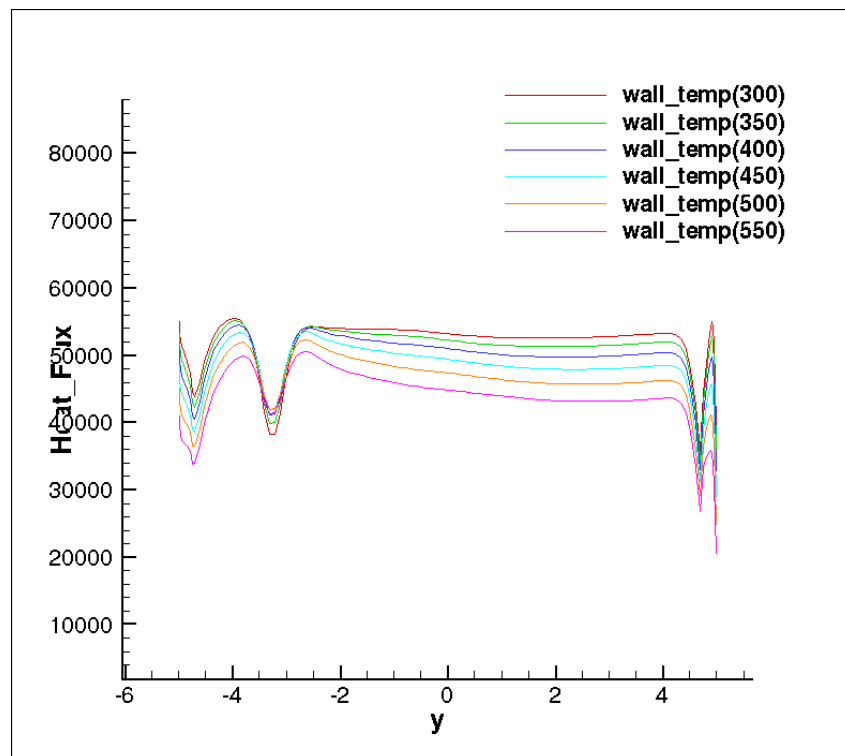
From the Fig: 3.45 we can see that when the wall temperature of the re-entry vehicle increases the heat flux is decreases. This is because when the wall temperature increases, the temperature difference between fluid and surface decreases and thus the heat flux decreases.

Chapter 4
Conclusions

Aerothermodynamics analysis of NASA's Orion crew exploration vehicle(CEV) re-entry vehicle investigated numerically at low altitude of the earth. At low altitude continuum approximation is valid due to high density region. The Favre averaging (density weighted averaging) procedure is applied to obtain the governing equations. The Favre averaged Navier-stokes along with Spalart-Allmaras turbulent model are used to compute flow field in high density region using open source finite volume based CFD code SU2. The Pointwise software was used for meshing and the SU2 software was used for the numerical simulations. The following conclusions are derived from the present investigation:

- The bow shock formation is observed in front of re-entry (blunt) vehicle due to supersonic flow.
- With increase in free stream Mach number the bow shock strength increases and also forms closer to the surface.
- The surface heat flux and surface pressure increases with increase in free stream Mach number.
- The surface heat flux increases at the nose center region due to shock /boundary layer interactions.
- The flow filed significantly changes at the edge of re-entry vehicle due to merging of bow shock and expansion waves.
- The stagnation point and maximum surface pressure location changes with respect to angle of attack.
- The surface heat flux decreases with increase of surface temperature due to decrease of temperature difference between fluid and surface.
- Present simulations are able to capture flow field characteristics such as bow shock and shock/ boundary layer interactions. Hence Present results would be useful for design and development of re-entry vehicles.

Chapter 5

Scope for future work

Procedure used in this work for Orion CEV re-entry vehicle can be further used to study of other re-entry vehicles and also ballistic missiles. Present results of high density regime would be useful for design of thermal protection system (TPC) of Orion CEV re-entry vehicle. Generally TPC to re-entry vehicle at high temperature and high heat flux is provided in terms of ablative material coating. An ablation code can be developed to predicate optimize thickness of the ablative material for safety of re-entry vehicle against high thermal load.

References

[1] Geogory P. Kennedy. Vegeance Weapon 2: The V-2 Guided missile. Smithsonian Insition press 1983.

[2] Dennis R. Jenkins, Tory Landies and Jay Miller. American X-Vehicles: An Inventory X-1 to X-50. June 2003.

[3] L Robert, O Neal and Leonard Rabb. Heat shield performance during atmospheric Entry of project mercury Research and Development Vehicle NASA. May 1961.

[4] Barton C. Hacker and James M. Grimwood. On the shoulders of Titans: A History of project Gemini. NASA SP-4206,1977.

[5] Robert O.Pillar and Caldwell J. Johnson. Johnson Apollo spacecraft Design. , NASA Industry Apollo Technical Conference: A Compilation of the papers presented July 1961; 18-20.

[6] Anon. NASA's exploration systems architecture study, final report. NASA TM-2005-214062, November 2005.

[7] H. J. Allen . Hypersonic Flight and the Reenty Problem. Journal of the Aeronautical Sciences, 1958;25: 217-230.

[8] A. J. Eggers Performance of Long Range Hyper velocity Vehicles. Jet Propulsion, 1958; 27: 1147-1151

[9] T. A. Heppenheimer. Facing the Heat Barrier: A History of Hypersonics. The NASA History Series, September 2007

[10] John J. Bertin and Russell M. Cummings. Fifty years of hypersonic: where were been, where were going. Journal of Progress in Aerospace Sciences 2003; 39:511-536.

[11] Moretti G. and M. Abbett. A Time-Dependent Computational Method for Blunt Body Flows AIAA J. December 1966; 4(12): 2136-2141.

[12] Brian R. Hollis and Salvaore Borrelli. Aerothermodynamics of blunt body entry vehicles. Journal of Progress in Aerospace Sciences 2012;48-49:42-56.

[13] A. Viviani, G. Pezzella. Computational flow field analysis over a blunt-body re-entry vehicle. Journal of Spacecraft and Rockets 2010; 47(2): 258-270.

[14] Giuseppe Pezzella. Aerodynamic and aerothermodynamic trade-off analysis of a small hypersonic flying test bed. Journal of Acta Astronautica 2011; 69:209-222.

[15] Fulvio Stella, Marilena Giangi, Fabio Paglia, Marco Dascenzi and Marco Iannuccelli. Numerical Simulation of Re-Entry Flow: Heat Flux Evaluation. Journal Heat transfer Engineerin, Taylor and Francis 2006; 27(2):58-69.

[16] Guiseppe Pezzella. Hypersonic environment assessment of the CIRA FTB-X re-entry vehicle. Journal of Aerospace Science and Technology March 2013;25(1):190-202.

[17] Kunihiko Ohtake. Thermal analysis of the thermal protection system for the re-entry vehicle. Computers methods in applied mechanics and science 1998; 151:301-310.

[18] Raffaele Savino, Mario De Stefano Fumo, Diego Paterna and Michelangelo Serpico. Aerothermodynamics study of UHTC-based thermal protection systems. Journal of Aerospace science and Technology 2005;9:151-160.

[19] Rakeshkumar K. Patel and K. Venkatasubbaiah, Numerical Simulation of the Orion CEV Reentry Vehicle, Journal of Aerospace Engineering, 2015, 28(2): 04014067-1-8.

[20] Saric WS, Muylaert J and Dujarric C. Hypersonic experimental and computational capability, improvement and validation. AGARD A R-319 May 1966; vol.1.

[21] R. L. Kruse. Transition and flow reattachment behind an Apollo like body at Mach numbers to 9. NASA TN D-4645,1968.

[22] B. R. Hollis, K. T. Berger, T. J. Horvath, J.J. Coblish, J. D. Norris, R. P. Lillard, etal. Aeroheating testing and predictions for project Orion Crew Exploration. Journal of Spacecraft and Rockets 2009; 46(4): 76680.

[23] K. Sinha and D.K. Reddy Hypersonic turbulent flow simulation of FIRE *11* re-entry vehicle afterbody. Journal of Spacecraft and Rockets 2009, 46(4):2009.

[24] Muylaert J, Kumar A and Dujarric C. Hypersonic experimental and computatuinal capability, improvement and validation. AGARD AR-319 May 1998; vol *11*.

[25] Raffaele Votta, Antonio Schettino and Aldo Bonfiglioli. Hypersonic high altitude aerothermodynamics of a space re-entry vehicle. Journal of Aerospace science and Technology March 2013;25(1):190-202.

[26] John D. Anderson Hypersonic and High-Temperature Gas dynamics. 2nd edition. AIAA Education series 2006.

[27] W. G. Vincenti and C.H. Kruger. Introduction to Physical Gas Dynamics. Wiley New York, 1965.

[28] Domenic D Abrosio. A study on Shock Wave Boundary layer Interaction in High-Speed Flows. 4th Europ Symp. Aerothermodynamics for Space Applications, Capula, Italy. ESA Sp-48 2002; 733-741.

[29] US Standard atmosphere 1976. National oceanic And Atmospheric Administration, National Aeronautical and Space Administration and US Air Force 1976.